

A description of a *Denazinemys nodosa* specimen (Testudinata, Baenidae) from the Late Cretaceous Kaiparowits Formation of southern Utah

Gaël E. Spicher^{1,2}, Joseph J. W. Sertich^{3,4}, Léa C. Girard¹, Walter G. Joyce¹, Tyler R. Lyson⁵, Yann Rollot¹

¹ Department of Geosciences, University of Fribourg, 1700 Fribourg, Switzerland

² Institute of Geosciences, Section Paleontology, Rheinische Friedrich-Wilhelms-Universität Bonn, Nußallee 8, 53115 Bonn, Germany

³ Department of Geosciences, Warner College of Natural Resources, Colorado State University, Fort Collins, Colorado, USA

⁴ Smithsonian Tropical Research Institute, Panama City, Panama

⁵ Department of Earth Sciences, Denver Museum of Nature & Science, Denver, Colorado, USA

<https://zoobank.org/A97F2AE5-019E-46D2-9B7B-584CB48CAFE0>

Corresponding author: Gaël E. Spicher (spicher.gael@gmail.com)

Academic editor: Florian Witzmann ♦ Received 22 February 2023 ♦ Accepted 14 June 2023 ♦ Published 31 July 2023

Abstract

Denazinemys nodosa is a Late Cretaceous representative of the North American turtle clade Baenidae diagnosed, among others, by a shell surface texture consisting of raised welts. We provide a detailed description of a partial skeleton from the late Campanian Kaiparowits Formation of Utah, USA, including bone-by-bone analysis of its cranium based on images obtained using micro-computed tomography. A revised phylogenetic analysis confirms placement of *Denazinemys nodosa* close to *Eubaena cephalica* and *Boremys* spp. within the clade Eubaeninae. Comparison with a second skull from the Kaiparowits Formation previously assigned to *Denazinemys nodosa* questions its referral to this taxon. An assortment of specimens from the Early to Late Campanian of Mexico and the USA had previously been referred to *Denazinemys nodosa* based on shell surface texture alone, even though this characteristic is known to occur in other baenids. Our review of all available material concludes that *Denazinemys nodosa* is currently only known from the Late Campanian of New Mexico and Utah.

Key Words

Baenidae, Baenodda, Campanian, Kaiparowits Formation, Late Cretaceous, Paracryptodira, Testudinata, Utah

Introduction

Baenidae is a clade of typically riverine paracryptodiran turtles that lived in North America from the Early Cretaceous to Eocene (Joyce and Lyson 2015). A conspicuous representative of the clade, easily diagnosed even in the field by the nodular surface texture of its shell, is *Denazinemys nodosa* (Gilmore, 1916). To date, well diagnosed material has been recovered from the Late Campanian of the Fruitland and Kirtland formations of New Mexico (Gilmore 1916, 1919; Wiman 1933; Lucas and Sullivan 2006; Sullivan et al. 2013; Dalman and

Lucas 2016; Lichtig and Lucas 2017) and the Kaiparowits Formation of Utah, USA (Hutchison et al. 2013; Lively 2016). Although this taxon was historically only known from shells, two skulls were recently reported and briefly described from the Kaiparowits Formation of Utah (Lively 2016).

Over the course of the last several decades, X-ray micro-computed tomography (μ CT) has proven itself essential in yielding novel insights into the cranial anatomy of turtles (e.g., Brinkman et al. 2006, 2009; Sterli et al. 2010), including baenids (Lipka et al. 2006; Rollot et al. 2018, 2022a, b; Evers et al. 2021), as this method provides a

non-destructive means to visualize structures hidden from external view and evaluate cryptic interelement sutures. As the above-mentioned skulls of *Denazinemys nodosa* are expected to provide additional insights into the taxonomy, phylogenetic relationships, and ecology of this turtle, we here provide a detailed description of one of them (DMNH EPV.64550) based on μ CT scans. We also provide a more detailed description of its shell based on 3D surface scans. These novel insights are then utilized to update the diagnosis of this turtle, to provide a novel phylogenetic hypothesis of baenid relationships, and to highlight possible paleoecological and paleogeographic implications. A difficult issue with which we were confronted during this study is the apparent differences between DMNH EPV.64550 and the second available skull of *Denazinemys nodosa* (BYU 19123), which cannot be explained satisfactorily for the moment.

Institutional abbreviations: BYU, Brigham Young University, Provo, Utah, USA; DMNH, Denver Museum of Nature & Science, Denver, Colorado, USA.

Materials and methods

Geologic setting

Specimen DMNH EPV.64550 was recovered from the middle unit of the Kaiparowits Formation (DMNH Loc. 4418), within the central Kaiparowits Plateau of Grand Staircase-Escalante National Monument, southern Utah (Fig. 1). The locality is approximately 200–300 meters above the lower contact with the Wahweap Formation, located stratigraphically higher than Ash Bed KP-07 of Roberts et al. (2013), U-Pb dated to 76.394 ± 0.040 Ma, and below Ash Bed KBC-109, dated to 75.609 ± 0.015 Ma (Ramezani et al. 2022), thus placing the locality at approximately 76 Ma. The youngest certain occurrence of *Denazinemys nodosa*, the type locality in the De-Na-Zin Member of the Kirtland Formation, is capped by Ash J (Fassett and Steiner 1997), dated to 73.496 ± 0.039 Ma (Ramezani et al. 2022). This established stratigraphic range for the taxon, between ~ 76 Ma and ~ 73.5 Ma is potentially extended by fragmentary remains recovered from older units in the southern portion of the Western Interior, including the Lower Shale Member of the Aguja Formation (~ 80 – 77 Ma; Lehman et al. 2019), the Allison Member of the Menefee Formation (~ 83 – 80 Ma; Lichtig and Lucas 2015), and the Coyote Point Member of the Wahweap Formation (~ 81 – 80 Ma; Holroyd and Hutchison 2016; Beveridge et al. 2022). However, none of this material is necessarily diagnostic of *Denazinemys nodosa* per se, as other turtles from the Campanian are known to have a nodular surface texture, such as *Boremys* spp. and *Scabremys ornata* (Gilmore 1935; Sullivan et al. 2013, see Discussion below).

In addition to the associated shell and skull of *Denazinemys nodosa* (DMNH EPV.64550), fossil specimens recovered from DMNH Loc. 4418 include a small partial dentary of the alligatoroid c.f. *Brachychampsa*

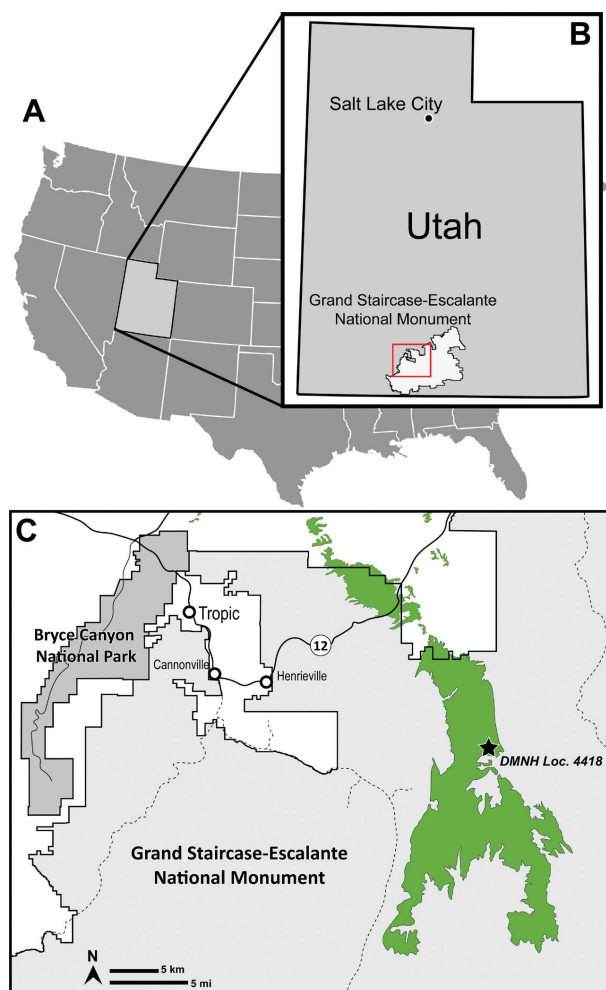


Figure 1. Map showing the location of DMNH Loc. 4418 on the Kaiparowits Plateau of Grand Staircase-Escalante National Monument, southern Utah, U.S.A. (A), with inset of Utah (B), and the location of the main exposures of the Kaiparowits Formation in and around Grand Staircase-Escalante National Monument (C). Green areas represent aerial exposure of the Kaiparowits Formation.

sp. and rounded fragments of other turtle taxa typical of aquatic assemblages in the Kaiparowits Formation. The sediment at the locality consists of a fine-grained, sandy mudstone associated with overbank floodplain deposition in a ponded setting (Facies Association 8 of Roberts [2007]). Shell elements were disarticulated and chaotically oriented in an area of less than $\frac{1}{4}$ square meter, with many elements cleanly broken prior to, or during, deposition. Breaks of shell elements ranged from mild offsets to widely scattered pieces, with some portions of individual elements recovered from different sides of the association and later repaired in the laboratory. This suggests the pre-depositional disarticulation of an individual, possibly at the bottom of a shallow pond, followed by a higher energy depositional event (e.g., flood, avulsion) that rearranged and disturbed elements but did not carry them far before final deposition. The skull was found within the cluster of chaotically arranged shell elements, surrounded by portions of shell within the sediment. All shell elements

referred to *D. nodosa* from the site are consistent in size and preservation. This, combined with the absence of duplicated elements, strongly suggests that the locality preserved only one individual of *D. nodosa* and that the closely associated skull can be confidently assigned to the same individual. Smaller elements, including appendicular elements, vertebrae, and mandibles, may have been lost to winnowing during deposition or scavenged, though the remaining elements do not show evidence of scavenging by a large-bodied vertebrate such as a crocodyliform or non-avian theropods.

Visualization

μCT-scan: We used high-resolution X-ray micro-computed tomography to obtain the internal cranial morphology of DMNH EPV.64550. The scan was undertaken at the University of Texas High-Resolution X-ray Computed Tomography Facility in Austin, Texas, USA with a NSI scanner with 3600 projections, a voltage of 180 kV, a current of 160 μA, and an aluminum filter. The projections were converted into 1930 coronal slices with a voxel size of 33.1 μm. To generate and visualize the bones and canals of DMNH EPV.64550 in three dimensions, we used the software program Amira (version 6.1.1; <https://www.thermofisher.com/>). We utilized the brush and lasso tools of Amira to manually highlight the boundaries of all bones and canals preserved in the specimen in every third slice in the x-axis. The reconstructions were then obtained through interpolation using the appropriate tool. Isosurface models were exported as .ply files. The visualization of the 3D models was made in the software Blender (version 2.79b; <https://www.blender.org>). The image stack and the 3D models are available at Morphosource (<https://www.morphosource.org/projects/000483670>).

Surface scanning: The carapace and plastron of DMNH EPV.64550 were scanned using a portable surface scanner Artec Space Spider at DMNS. The scans were acquired and treated with the software Artec Studio 16 Professional: scans from different angles were performed to acquire the full 3D morphology of each shell part, each scan was cleaned, landmarks were manually applied to align and fuse scans, and holes automatically filled to produce a single, watertight 3D model. Models were exported as .obj files with an associated texture as .png file. The models were later loaded into MeshLab to merge mesh and texture on a single .ply model for each piece of the shell. The 3D models are available at Morphosource (<https://www.morphosource.org/projects/000483670>).

Phylogenetic analysis

To explore the phylogenetic relationships of *Denazinemys nodosa* with other baenids, we modified the character/taxon matrix of Rollot et al. (2022b). We utilized the herein new observations to score the cranial anatomy of

Denazinemys nodosa, thereby partially replicating the efforts of Lively (2016) in capturing the cranial anatomy of this taxon. The previously existing postcranial scorings for this taxon were updated by reference to the shell of DMNH EPV.64550, in particular characters 35 (preneural; 0/1 [variously present], not ?), 48 (placement of anal scutes; 1 [z-shaped], not 0), 49 (xiphiplastron/hypoplastron suture; 1 [z-shaped], not ?), 88 (proportions of neural V; 1 [longer than wide], not ?), and 89 (neural VI contacts; 1 [contacts costals V, VI, and VII], not ?). We furthermore updated the scoring of *Goleremys mckennai* by reference to Hutchison (2004), as this taxon was deemed to be problematic by some previous analyses (e.g., Lyson and Joyce 2010; Lyson et al. 2019), in particular characters 63 (parietal width versus length; 1 [combined width greater than length], not ?), 73 (size of external narial opening; 0 [much smaller than orbit], not ?), 96 (basipterygoid processes; 2 [absent], not ?), and 101 (bones contributing to occipital condyle; 1 [basiooccipital only], not ?). The final matrix consists of 105 characters scored for 48 taxa and can be found in Suppl. material 1.

The matrix was subjected to a parsimony analysis using TNT (Goloboff et al. 2008). Unless stated otherwise, we used the default settings. Characters 5, 9, 13, 15, 17, 25, 26, 29, 32, 37, 38, 39, 44, 46, 58, 61, 78, 86, 93, 95, 96, 99 (here and elsewhere, we are not using the numeration of TNT) form morphoclines and were ordered. 1,000 replicates of random addition sequences were followed by a second round of tree bisection-reconnection. As we are doubtful about the common presence of 12 peripherals in baenodds (see Discussion), we deactivated character 36, which captured its purported distribution across the ingroup. We furthermore deactivated character 57 (presence of horizontal tubercles of the basiooccipital), as we are unable to replicate its current meaning or coding.

Systematic paleontology

Testudinata Klein, 1760 (Joyce et al., 2020a)
Paracryptodira Gaffney, 1975 (Joyce et al., 2021)
Baenidae Cope, 1873 (Joyce et al., 2021)
***Denazinemys* Lucas & Sullivan, 2006**

***Denazinemys nodosa* (Gilmore, 1916)**

Holotype. USNM 8345, an almost complete shell (Gilmore 1916, figs 34, 35, pl. 76; Sullivan et al. 2013, fig. 20.2a, b).

Type locality and horizon. Locality 60, Willow Wash, 2 miles northwest of Ojo Alamo store, San Juan County, New Mexico (Gilmore 1916), USA; De-na-zin Member, Kirtland Formation, upper Campanian, Upper Cretaceous (Sullivan et al. 2013).

Referred material and range. Upper Cretaceous (Campanian) Fruitland and Kirtland formations of New Mexico (Gilmore 1916, 1919; Wiman 1933; Lucas and Sullivan 2006; Sullivan et al. 2013; Dalman and

Lucas 2016; Lichtig and Lucas 2017) and Kaiparowits Formation of Utah (Hutchison et al. 2013; Lively 2016) (see Discussion for justification).

Revised diagnosis. *Denazinemys nodosa* can be identified as a representative of Baenodda by the contribution of vertebral V to the posterior margin of the shell, an omega-shaped femoral-anal sulcus, and a midline contact between both extragulars posterior to the gulars and a representative of Eubaeninae by the presence of a subdivided cervical, the presence of prepleurals, and a vertebral III that is longer than wide. Among eubaenines *Denazinemys nodosa* can be differentiated by the following combination of characters: presence of welt-like ornamentation on the carapace (also present in *Boremys* spp. and *Scabremys ornata*), absence of a posterodorsal extension of the quadratojugal that crests the cavum tympani (also absent in *Baena arenosa* and *Chisternon undatum*), the presence of epipterygoids, large mandibular condyles, and a nasal/frontal suture that is anteriorly convex (Joyce and Lyson 2015).

Description. General. The cranium is generally well preserved, despite minor crushing mainly affecting the right side of the specimen (Figs 2, 3). The right quadratojugal and right squamosal are missing. Portions of the right quadrate and paroccipital process of the right opisthotic dislocated from the remainder of the cranium but are preserved as an articulated fragment that was μ CT scanned together with the skull, though not in the position it was originally found. The sutures of the cranium can be distinguished with relative ease in the μ CT scan. The skull is about 65 mm long from the anterior tip of the nasals to the posterior end of the supraoccipital crest, and 48 mm wide between the outside edge of the mandibular condyles. The skull is wedge-shaped in dorsal view and possesses a distinct, pinched snout (Fig. 2A). The less deformed left side suggests that the orbits were oriented dorsolaterally. The upper temporal emargination protrudes anteriorly beyond the level of the anterior margin of the cavum tympani (Fig. 2B). The last three observations are in broad agreement with other baenodds (Joyce and Lyson 2015). The dorsal skull roof is decorated with fine crenulations, but distinct scute sulci appear to be absent.

Nasal. The nasals are flat and narrow elements that roof the nasal cavity (Fig. 2). In dorsal view, the nasal is longer than broad and contacts its counterpart medially and the frontals posteriorly and posteromedially. The nasal is prevented from contacting its counterpart for nearly half of its length posteriorly by an anterior extension of the frontal (Fig. 2A). This anterior process of the frontal also covers the posteromedial aspect of the nasal. Within the nasal cavity, the nasal contacts the prefrontal posterolaterally, but such a contact is prevented externally by an extended contact between the frontal and maxilla (Fig. 2C, E). On the uncrushed, left side of the skull, the apertura narium externa forms a posteriorly oriented slit starting from its dorsolateral margin. The slit extends posteriorly and reaches the frontal, thus preventing the nasal from contacting the maxilla (Fig. 2A). As

preserved, the right nasal contacts the right maxilla along a straight contact, but deformation in combination with a lack of apparent articulation sites suggest that this is due to compression. The nasal of *Denazinemys nodosa*, therefore, differs from the more elongated nasal that contacts the maxilla of *Eubaena cephalica* (Gaffney 1972; Rollot et al. 2018), *Goleremys mckennai* (Hutchison 2004), and *Saxochelys gilberti* (Lyson et al. 2019).

Prefrontal. The prefrontals are well preserved despite some shearing on both sides. The dorsal plate is greatly reduced in size as in the majority of baenodds (Joyce and Lyson 2015). The dorsal plate of the prefrontal is developed as a small, rectangular lappet that forms the anterodorsal margin of the orbit (Fig. 2A, C, E). The dorsal process of the prefrontal contacts the maxilla anteriorly and the frontal dorsally and posteriorly. The dorsal process furthermore contacts the nasal within the roof of the nasal cavity, as in *Eubaena cephalica* (Rollot et al. 2018). The descending process of the prefrontal frames the orbit anteriorly and forms the anterior margin of the foramen interorbitale and the anterior half of the foramen orbito-nasale, which is posteriorly framed by the palatine. Anteriorly, the descending process of the prefrontal broadly contacts the maxilla ventrolaterally along a straight suture, the vomer posteroventrolaterally, and the palatine on both sides of the foramen orbito-nasale. A blunt, sheet-like ridge along the medial aspect of the descending process of the prefrontal might be apparent on the right side, but a constriction of the fissura ethmoidalis as that observed in some early branching baenids is not apparent in *Denazinemys nodosa* (Rollot et al. 2022a).

Frontal. The frontal is a flat and elongate element, trapezoidal in dorsal view, mediolaterally wider posteriorly than anteriorly (Fig. 2A, C–E). The frontal contacts the nasal anteriorly along a deeply concave suture, the maxilla anterolaterally, the dorsal process of the prefrontal lateroventrally, the postorbital posterolaterally, the parietal posteriorly, and its counterpart medially for its entire length. The frontoparietal suture is located posterior to the orbit. The left frontal likely has a minute contribution to the posterior margin of the slit-like opening located between the nasal and maxilla, which had previously not been noted (Lively 2016). The frontal bears a pointed anterior process that deeply protrudes between the nasals, preventing the latter to contact one another along their posterior half. At about two thirds of its length, the frontal is slightly expanded laterally to form the dorsal margin of the orbit (Fig. 2C, E). Ventrally, the frontal is thickened to form a low crista cranii that separates the orbit from the low but broad sulcus olfactorius. The crista cranii is not continuous with the parietal posteriorly.

Parietal. The parietals are complete but slightly damaged, mostly along the ventral aspect of their descending process (Fig. 2A). The parietal forms the anteromedial wall of the temporal fossa, the posterior margin of the foramen interorbitale, and the anterior and medial margin of the upper temporal emargination. The dorsal part of the parietal forms a thin plate of bone

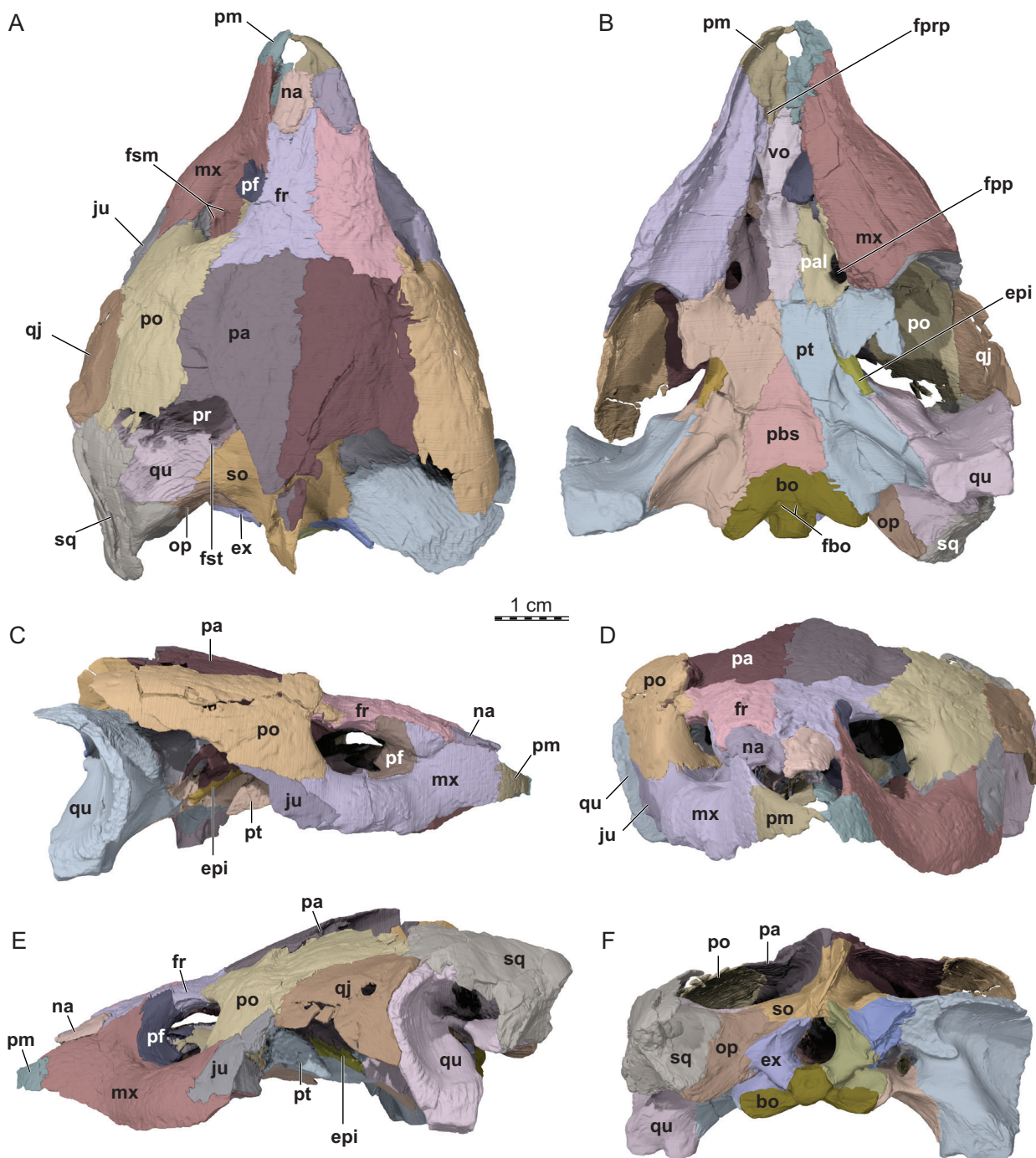


Figure 2. Skull of *Denazinemys nodosa* (DMNH EPV.64550), Late Cretaceous (Campanian) of southern Utah, U.S.A. Three-dimensional renderings of the skull in: **A.** Dorsal; **B.** Ventral; **C.** Right lateral; **D.** Anterior; **E.** Left lateral, and **F.** Posterior views. Abbreviations: bo, basioccipital; epi, epipterygoid; ex, exoccipital; fbo, foramen basioccipitale; fpp, foramen palatinum posterius; fprp, foramen praepalatinum; fr, frontal; fsm, foramen supramaxillare; fst, foramen stapedio-temporale; ju, jugal; mx, maxilla; na, nasal; op, opisthotic; pbs, parabasisphenoid; pa, parietal; pal, palatine; pf, prefrontal; pm, premaxilla; po, postorbital; pr, prootic; pt, pterygoid; qj, quadratojugal; qu, quadrate; so, supraoccipital; sq, squamosal; vo, vomer.

that is slightly broader anteriorly than posteriorly, but the combined width of the parietals is about as great as their length. The dorsal plate contacts the frontal anteriorly, the postorbital laterally, the supraoccipital posteriorly, and its counterpart medially. Within the upper temporal fossa, the vertical process of the parietal, or processus inferior parietalis, contacts the prootic laterally and the supraoccipital

posteriorly. A distinct ridge extends posteroventrally along the lateral surface of the processus inferior parietalis, starting from the contact with the postorbital to nearly reach the ventral contact with the epipterygoid. Within the lower temporal fossa, the processus inferior parietalis contacts the pterygoid anteroventrally, the epipterygoid ventrally, again the pterygoid posteroventrally along the

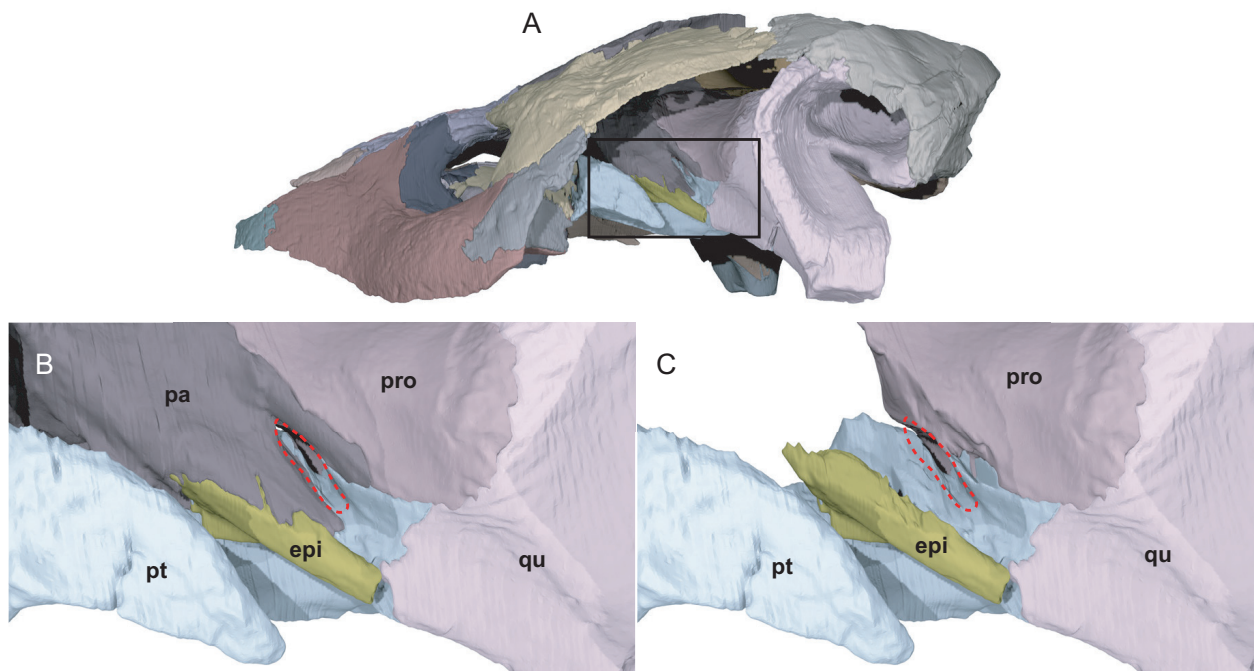


Figure 3. Three-dimensional renderings of the left trigeminal foramen of DMNH EPV.64550. **A.** Left lateral view of DMNH EPV.64550 showing the area of interest; **B.** Close-up on the left trigeminal foramen area highlighting its external margin; **C.** Close-up on the left trigeminal foramen area showing its internal margin. The margins of the trigeminal foramen are highlighted by the dashed red circles. Abbreviations: epi, epipterygoid; pa, parietal; pro, prootic; pt, pterygoid; qu, quadrate.

posterior margin of the foramen nervi trigemini, and the prootic posteriorly (Fig. 3). Within the braincase, the processus inferior parietalis additionally contacts the parabasisphenoid posteroventrally. Two finger-like processes of the parietal frame the anteroventral and posterodorsal margins of the trigeminal foramen and, independently from one another, contact the pterygoid ventrally. Although these contacts prevent the prootic from contributing to the external margin of the foramen nervi trigemini, as is the case in *Boremys pulchra* (Brinkman and Nicholls 1991), the prootic roofs the latter foramen from the inside, similar to the condition observed in *Lakotemys australodakotensis* (Rollot et al. 2022a). The parietal and epipterygoid jointly form a thickened ridge that runs diagonally from the dorsal skull roof to the articular surface of the quadrate just anteroventrally to the trigeminal foramen (Fig. 2B, C and E).

Postorbital. Despite some fractures, both postorbitals are overall well preserved. The anterior part of the postorbital is ventrally expanded as a mediolaterally thickened septum orbitotemporale (sensu Evers et al. 2020) that forms the posterior aspect of the fossa orbitalis and broadly rests on the jugal dorsally (Fig. 2A–E). The resulting, posteriorly constricted opening between the orbit and temporal fossa resembles the condition observed in other paracryptodires, but also pleurodires (Evers et al. 2020). Within the orbit, the postorbital mainly contacts the jugal ventrally, but additional contacts can be identified along the most posterior aspect of the orbital floor with the

maxilla anterolaterally and the pterygoid posterolaterally (Fig. 2B, C, and E). Along the posteroventral corner of the right orbit, the postorbital contacts the maxilla anteroventrally, which prevents the jugal from contributing to the orbital margin. On the left side, small portions of the jugal are inserted between the postorbital and maxilla in some areas (Fig. 2D). These repeated slight exposures of the jugal are somewhat unusual in comparison to other paracryptodires that either lack a jugal contribution to the orbital margin, or exhibit a clear jugal contribution to that margin. The condition exhibited on the left side likely corresponds to a preservational artefact, and we interpret the bony arrangement on the right side as being correct (Fig. 2A and D). A contact between the maxilla and postorbital along the posteroventral margin of the orbit was also reported in *Boremys pulchra* (Brinkman and Nicholls 1991), *Eubaena cephalica* (Gaffney 1972; Rollot et al. 2018), and *Saxochelys gilberti* (Lyson et al. 2019).

The posterior part of the postorbital is developed as a flat and elongate piece of bone (Fig. 2). Although the posterior margin of both postorbitals is damaged, the intact margins of the surrounding elements strongly suggest that the postorbital broadly contributed to the upper temporal emargination. On the skull roof, the postorbital contacts the frontal anteromedially, the parietal medially, the jugal anterolaterally, the quadratojugal laterally, and the squamosal posterolaterally.

Jugal. The jugals are both damaged and their posterior portion is not preserved (Fig. 2C and E). The jugal

is a small element that forms the anterodorsal margin of the cheek emargination. The right jugal preserves a small portion of that margin, indicating that the cheek emargination likely reached the level of the ventral margin of the orbit at the most. In lateral view, the jugal contacts the maxilla anteriorly and anteroventrally and the postorbital dorsally. A contact with the quadratojugal posteriorly is preserved on the left side only (Fig. 2E). The jugal forms a thick process medially that lies beneath the postorbital and is partially exposed within the orbit, where it contacts the maxilla anteriorly and medially along a V-shaped suture. The jugal contacts the postorbital dorsally. A small exposure of the jugal is apparent on the left side (Fig. 2A, D), but this is likely due to some damage or shearing, and the bony arrangement along the posteroventral corner of the right orbit appears to be the usual condition for DMNH EPV.64550 (see Postorbital above). Within the lower temporal fossa, the medial process of the jugal contacts the pterygoid posteromedially, anterior to the external process of the latter (Fig. 2B).

Quadratojugal. Only the left quadratojugal is preserved in DMNH EPV.64550 (Fig. 2A, C, and E). The quadratojugal is a flat, subtriangular element that forms the posterodorsal margin of the lower temporal emargination. The quadratojugal contacts the jugal anteriorly, the postorbital dorsally, the squamosal posterodorsally, and the quadrate posteriorly (Fig. 2E). A contribution of the quadratojugal to the margin of the cavum tympani is not apparent.

Squamosal. The right squamosal is missing in DMNH EPV.64550, but its left counterpart is entirely preserved, albeit crossed by various fractures (Fig. 2A, B and E, F). The squamosal forms the posterodorsal aspect of the skull and contributes to the posterodorsal rim of the cavum tympani, the posterolateral margin of the upper temporal emargination, and the posterior and lateral margins of a deep antrum postoticum (Fig. 2E). On the skull roof, the squamosal contacts the quadratojugal anterolaterally and the postorbital anteromedially, and broadly contacts the quadrate ventrally. Within the upper temporal fossa, the squamosal contacts the quadrate anteromedially and the paroccipital process of the opisthotic medially (Fig. 2A, F). The squamosal broadly covers the posterodorsolateral aspects of the quadrate to form a deep antrum postoticum. The ridge that runs from the posterior tip of the squamosal towards the paroccipital process is damaged on the left side of the skull. As a result, the pit behind the antrum postoticum, best seen in lateral view (Fig. 2E), for attachment of the *M. depressor mandibulae* is incomplete.

Premaxilla. The premaxilla forms the floor of the fossa nasalis and the ventral margin of the apertura narium externa (Fig. 2A–E). The premaxillae are visible in dorsal view, as in other eubaenines. The premaxilla contacts the vomer posteriorly, the maxilla posterolaterally, and its counterpart medially. The premaxillae form a relatively large, rounded opening along their median suture that resembles the intermaxillary foramen of trionychians (Fig. 2A, B). This foramen, perhaps the result of taphonomic damage, is not homologous with the foramen praepalatinum, as the latter

is preserved along the most posterior aspect of the premaxilla. The foramen praepalatinum is mostly formed by the premaxilla, with contributions of the maxilla posterolaterally, as in *Eubaena cephalica* (Gaffney 1972; Rollot et al. 2018) but not other eubaenines for which this area is known (Gaffney 1972; Hutchison 2004). The premaxilla forms the anterior aspects of the labial margin, contributes only little to the triturating surfaces, and defines a distinct median tongue groove, much as in *Stygiochelys estesi* (Gaffney and Hiatt 1971), *Chisternon undatum* (Gaffney 1972), *Eubaena cephalica* (Gaffney 1972; Rollot et al. 2018), and *Saxochelys gilberti* (Lyson et al. 2019), but likely not *Goleremys mckennai* (Hutchison 2004). A lingual ridge is not present.

Maxilla. The maxilla forms the anterior and ventral margins of the orbit, the lateral margin of the apertura narium externa, the lateral wall of the fossa nasalis, minor aspects of the lateral margin of the foramen palatinum posterius, and floors the fossa orbitalis (Fig. 2A–E). The ascending process of the maxilla forms a thin sheet of bone bordered by the apertura narium externa anteriorly and the orbit posteriorly. The ascending process contacts the frontal dorsally and the prefrontal posteriorly. On the right side of the skull, the maxilla contacts the nasal, but this contact is likely due to shearing, as such a contact appears to be absent on the left. The maxilla contacts the premaxilla anteriorly. Within the fossa orbitalis, the maxilla contacts the descending process of the prefrontal anteromedially, the palatine medially, the pterygoid posteromedially, and the postorbital posterolaterally, and broadly underlies the jugal, which results in a V-shaped suture located just lateral for the foramen supramaxillare. The foramen is developed singularly on the right side, but is doubled on the left. In either case, the foramina are connected to a canal, that runs below the surface of the orbit and connects to a network of sub-canal that feed numerous nutritive foramina that are dispersed across the ventral side of the maxilla (Fig. 2B). The maxilla forms triturating surfaces that broaden posteriorly, as in *Stygiochelys estesi* (Gaffney and Hiatt 1971), *Eubaena cephalica* (Gaffney 1972; Rollot et al. 2018), *Boremys pulchra* (Brinkman and Nicholls 1991), *Goleremys mckennai* (Hutchison 2004), *Saxochelys gilberti* (Lyson et al. 2019), and *Palatobaena* spp. (Archibald and Hutchison 1979; Lyson et al. 2009; Lyson et al. 2021). Anteriorly, the triturating surface bears a distinct lingual ridge that delineates a broad tongue groove. The medial margin of the triturating surface is slightly thickened, but does not form a distinct ridge, much as in *Eubaena cephalica* (Gaffney 1972; Rollot et al. 2018). In ventral view, the maxilla contacts the premaxilla anteriorly, the vomer anteromedially, the palatine medially and posteromedially, and the pterygoid posteriorly.

Palatine. The palatine is a laminar bone that forms most of the foramen palatinum posterius and the posterior half of the foramen orbito-nasale (Fig. 2B). The palatine contacts the prefrontal anterodorsally, the vomer medially along a straight suture for most of its length, the maxilla ventrolaterally, and the pterygoid posteriorly.

The palatine only contributes minorly to the triturating surface. A contact with the jugal is absent, which differs from the condition observed in *Eubaena cephalica* (Rollot et al. 2018). The right palatine has a short contact with the descending process of the right parietal within the interorbital fossa, but such a contact is not present on the left side of the skull.

Vomer. The vomer is a single, elongated, and narrow bone (Fig. 2). The vomer floors the posterior part of the nasal cavity and forms the medial wall of the internal nares. The vomer contacts the premaxilla anteriorly, the maxilla anterolaterally, the prefrontal dorsolaterally, and the pterygoid posteriorly. The vomer also contacts the palatine laterally for most of its length, which prevents the latter from contacting its counterpart. The dorso-lateral processes of the vomer for articulation with the descending process of the prefrontals are very low, nearly nonexistent. Dorsally, a narrow sulcus vomeri is apparent along the posterior half of the bone.

Pterygoid. The pterygoids are well preserved with the exception of minor cracks. The anterior half of the pterygoid contacts the vomer anteromedially, the palatine anteriorly, the maxilla anterolaterally, and the jugal anterodorsolaterally (Fig. 2B, C, E). The pterygoid forms a reduced anterior process that barely protrudes between the vomer and palatine and extends only to the level of the posterior margin of the foramen palatinum posterius (Fig. 2B). Such a reduced anterior process contrasts with the elongate process of pleurosternids (Evers et al. 2020; Rollot et al. 2021) and early branching baenids (Evers et al. 2021; Rollot et al. 2022a; Rollot et al. 2022b), but resembles the condition of more derived baenids (Gaffney and Hiatt 1971; Gaffney 1972; Archibald and Hutchison

1979; Brinkman 2003; Hutchison 2004; Lyson and Joyce 2009a; Lyson and Joyce 2009b; Lyson and Joyce 2010; Lively 2015; Lyson et al. 2019; Lyson et al. 2021). The pterygoid forms a minor portion of the foramen palatinum posterius, which is apparent within its posterolateral corner. The pterygoid forms a well-defined external pterygoid process (Fig. 2C, E). The well-developed vertical flange has a broad contact with the overlying postorbital. The posterior half of the pterygoid has an elongate contact with the parabasisphenoid medially and the quadrate laterally (Figs 2B, 4). The pterygoid also contacts the basioccipital posteromedially for most of the length of the latter bone as in other baenids (Gaffney and Hiatt 1971; Gaffney 1972; Archibald and Hutchison 1979; Brinkman and Nicholls 1993; Brinkman 2003; Hutchison 2004; Lipka et al. 2006; Lyson and Joyce 2009a; Lyson and Joyce 2009b; Lively 2015; Lyson et al. 2019; Lyson et al. 2021; Rollot et al. 2022a; Rollot et al. 2022b) but which contrasts with the condition observed in pleurosternids (Evans and Kemp 1976; Gaffney 1979; Rollot et al. 2021). Posteriorly, the pterygoid forms a deep pterygoid fossa and the anterolateral half of the basioccipital tubercle. Within the lower temporal fossa, the pterygoid contacts the descending process of the parietal anterodorsally, the epipterygoid dorsally, and the prootic posterodorsally behind the foramen nervi trigemini, of which it forms the posterior margin (Fig. 3). The preserved portion of the pterygoid shows that the crista pterygoidea was likely low, but this area is difficult to assess given the shearing that is apparent in this area. Within the cavum acustico-jugulare, the pterygoid contacts the prootic anteriorly and anteromedially, the quadrate laterally, the exoccipital and basioccipital posteromedially. A contact with the processus

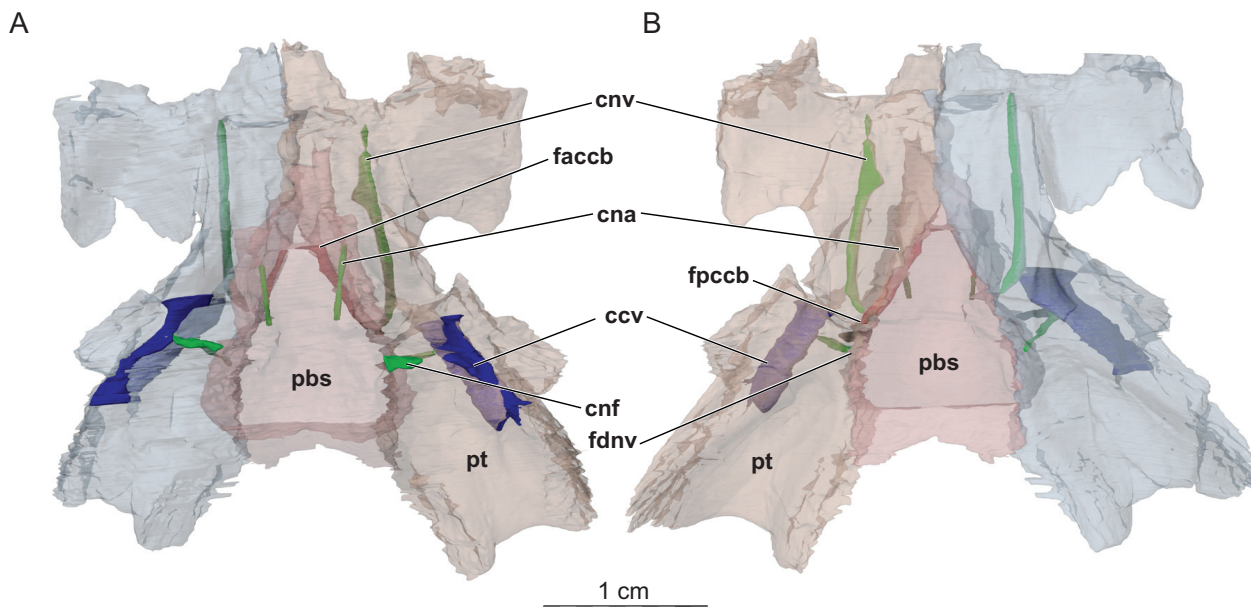


Figure 4. Three-dimensional renderings of the parabasisphenoid and the left and right pterygoids of the skull of *Denazinemys nodosa* (DMNH EPV.64550). **A.** Dorsal view and **B.** Ventral view of the bones rendered transparent showing the internal carotid artery and facial nerve systems. Abbreviations: ccv, canalis cavernosus; cna, canalis nervus abducentis; cnf, canalis nervus facialis; cnv, canalis nervus vidianus; faccb, foramen anterius canalis carotici basisphenoidalis; fdnv, foramen distalis nervi vidiani; fpccb, foramen posterius canalis carotici basisphenoidalis; pbs, parabasisphenoid; pt, pterygoid.

interfenestralis of the opisthotic was likely present dorso-medially as well, but can only partially be observed on the right side because of the shearing that affects the skull. The canalis cavernosus is mostly formed by the pterygoid and the prootic only forms the dorsal margin of the canal (Fig. 4). The foramen cavernosum is formed by the pterygoid and prootic and leads into the sulcus cavernosus anteriorly, which is formed by the pterygoid laterally and ventrally and minor contributions of the parabasisphenoid medially.

A short, anteroposteriorly oriented groove is located at about mid-length along the suture between the pterygoid and parabasisphenoid (Fig. 2B). This groove is inferred to have housed the internal carotid artery and two foramina can be identified along its posterolateral and anterior margins (Fig. 4). The posterolateral foramen is the foramen distalis nervi vidiani, which serves as a passage for the vidian nerve from the canalis pro ramo nervi vidiani to the carotid groove (Fig. 4). The foramen distalis nervi vidiani is formed by the pterygoid only, albeit located just lateral to the pterygoid-parabasisphenoid suture. The anterior foramen is the foramen posterius canalis carotici interni, which leads into the canalis caroticus internus. Just anterolateral to the foramen posterius canalis carotici interni, the canalis nervus vidianus bifurcates from the canalis caroticus internus and extends anteriorly through the pterygoid. The canalis nervus vidianus can be traced anteriorly close to the level of the suture between the pterygoid and palatine, just posterior to the foramen palatinum posterius, but crushing of the skull prevents us to determine the exact location and bony contributions to the foramen anterius canalis nervi vidiani. The canalis caroticus internus becomes the canalis caroticus basisphenoidalis just anterior to the split between the former canal and the canalis nervus vidianus, and extends anteromedially through the parabasisphenoid. The canalis caroticus basisphenoidalis joins the sella turcica by means of the foramen anterius canalis carotici basisphenoidalis, which is formed by the parabasisphenoid. The canalis caroticus lateralis, when present, typically extends anteriorly along the pterygoid-parabasisphenoid suture and joins the sulcus cavernosus. In DMNH EPV.64550, we are not able to identify any canal in this position, and the canalis caroticus lateralis is, therefore, considered absent in *Denazinemys nodosa*. The circulatory pattern of *Denazinemys nodosa* is overall very similar to that of *Eubaena cephalica* (Rollot et al. 2018), with the exception that the foramen distalis nervi vidiani is not ventrally exposed in *Eubaena cephalica*.

Epipterygoid. The epipterygoid is a small, rod-like bone, which is located anteroventral to the trigeminal foramen, but does not contribute to its formation (Figs 2B, C, E, 3). A notable ascending process is lacking. The epipterygoid contacts the pterygoid medially and ventrally and the parietal dorsally and anteriorly. A minor concavity at its posterior end marks remnants of the palatoquadrate cartilage (see Discussion for the known distribution of epipterygoids among baenodds).

Quadrate. The quadrate is a large bone that forms most of the middle ear, in particular the evenly rounded

cavum tympani, the medial aspects of the antrum postoticum, the posteriorly open incisura columella auris, the lateral wall of the cavum acustico-jugulare, and the mandibular condyle (Fig. 2). Within the upper temporal fossa, the quadrate contacts the prootic anteromedially, the supraoccipital medially, the opisthotic posteromedially, and the squamosal posteriorly (Fig. 2A). The contact between the quadrate and supraoccipital is extensive and prevents the opisthotic from contributing to the margin of the foramen stapedio-temporale, as in *Eubaena cephalica* (Rollot et al. 2018) and *Saxochelys gilberti* (Lyson et al. 2019), but not *Chisternon undatum* (Gaffney 1972) and *Stygiochelys estesi* (Gaffney 1972), in which the contact is either extremely reduced or completely absent, respectively. On the lateral skull surface, the quadrate forms a broad, C-shaped suture with the quadratojugal anteriorly and contacts the squamosal dorsally (Fig. 2E). In ventral view, the quadrate has an elongate contact with the posterior process of the pterygoid medially (Fig. 2B). An anterior contact with the epipterygoid is hindered by a rounded cavity that likely held the remnants of the palatoquadrate cartilage. The mandibular condyles are small, ventrally oriented, and consist of two concave facets, the lateral of which is larger than the medial one. The foramen stapedio-temporale is formed by the quadrate laterally, the prootic anteriorly, and the supraoccipital laterally and posterolaterally (Fig. 2A). The opisthotic has a minor contribution to the right canalis stapedio-temporalis internally, much as in *Eubaena cephalica* (Rollot et al. 2018). The quadrate and prootic also jointly form the processus trochlearis oticum, which is developed as a relatively broad ridge-like protrusion. Within the cavum acustico-jugulare, the quadrate contacts the prootic anterodorsomedially, the opisthotic posterodorsomedially, and the pterygoid ventromedially, and forms the lateral margin of the aditus canalis stapedio-temporalis.

Prootic. The prootic forms the medial half of the processus trochlearis oticum and the medial wall of the canalis stapedio-temporalis (Fig. 2A). The prootic is excluded from the lateral margin of the foramen nervi trigemini by a contact of the parietal with the pterygoid (Fig. 3B), but contributes to the foramen internally within the skull (Fig. 3C), as has previously been observed for *Lakotemys australodakotensis* (Rollot et al. 2022a). The prootic contacts the parietal anteriorly, the supraoccipital posteromedially, the quadrate posteriorly and posterolaterally, the pterygoid ventrolaterally, and the parabasisphenoid ventromedially. The prootic forms the anterior half of the cavum labyrinthicum, canalis semicircularis anterior, and canalis semicircularis horizontalis, and the anterior margin of the hiatus acusticus and fenestra ovalis. We are not able to determine if the fenestra ovalis is fully surrounded by bone because of damage to the processus interfenestralis of the opisthotic on both sides. The prootic also forms the dorsal margin of the canalis cavernosus and foramen cavernosum. The canalis nervus facialis extends laterally though the prootic from the fossa acustico-facialis and joins the medial margin of the

canalis cavernosus (Fig. 4). The geniculate ganglion, i.e. where the facial nerve splits into the vidian and hyoman-dibular nerves, is inferred to have been located within the canalis cavernosus. The canalis pro ramo nervi vidiani, which held the vidian nerve, extends ventromedially from the canalis cavernosus through the pterygoid and joins the carotid groove by means of the foramen distalis nervi vidiani. The vidian nerve is then inferred to have extended anteriorly alongside the internal carotid artery within the carotid groove into the canalis caroticus internus, and split from the latter to enter the canalis nervus vidianus just anterior to the foramen posterius canalis carotici interni. The canalis nervus vidianus is formed by the pterygoid.

Opisthotic. The opisthotics are damaged – the left lacks the processus interfenestralis and the right lacks most of the paroccipital process (Fig. 2A, B, F). The opisthotic forms the posterior margin of the hiatus acusticus and the posterior half of the cavum labyrinthicum, canalis semicircularis horizontalis, and canalis semicircularis posterior. Anteriorly, within the upper temporal fossa, the opisthotic contacts the supraoccipital medially and the quadrate laterally. A broad anterior contact with the prootic is hidden from dorsal view by a sheet of bone formed by the supraoccipital that laterally contacts the quadrate (Fig. 2A, F). The paroccipital process of the opisthotic forms the dorsal rim of the fenestra postotica, which is fully confluent with the foramen jugulare posterius, and contacts the exoccipital medially and squamosal laterally. The right opisthotic also slightly contributes to the posterior wall of the canalis stapedio-temporalis. Although the processus interfenestralis is absent on the left side and badly damaged on the right, we are able to assess most of its bony contributions. A contact with the pterygoid might have occurred ventrally, but the apparent contact on the right side seems to be the result of crushing. The foramen internum nervi glossopharyngei and foramen externum nervi glossopharyngei of the glossopharyngeal nerve (IX) are both preserved along the dorsal base of the processus interfenestralis. The processus interfenestralis forms the posterior margin of the fenestra ovalis but, as mentioned above (see Prootic), damage prevents us from determining if the fenestra ovalis was fully surrounded by bone. The processus interfenestralis also forms the dorsal margin of the foramen jugulare anterius, which is otherwise formed by the exoccipital and a small anterior contribution from the pterygoid. As preserved, the fenestra perilymphatica has a slit-like appearance, but this may be a result of compression.

Supraoccipital. The supraoccipital is complete, although some damage affects the crista supraoccipitalis, which is fragmented into two bony pieces (Fig. 2A, C, E, F). The supraoccipital forms the posteromedial tip of the skull roof, where it is only slightly exposed. The supraoccipital also forms the medial margin of the foramen stapedio-temporale, the dorsal margin of the hiatus acusticus, and the dorsal margin of the foramen magnum, and roofs the cavum cranii. The crista supraoccipitalis is moderately tall and thin and, despite some damage and slight displacement, appears to be complete, and the crista

barely protrudes beyond the level of the foramen magnum. The supraoccipital contacts the parietal anterodorsally, the prootic anterolaterally, the quadrate laterally, the opisthotic posterolaterally, and the exoccipital posteriorly. The supraoccipital roofs the cavum labyrinthicum and forms the posterior half of the canalis semicircularis anterior and the anterior half of the canalis semicircularis posterior. The foramen aqueducti vestibuli is not preserved.

Basioccipital. The basioccipital is an unpaired element that floors the posterior portion of the cavum cranii and forms the ventral margin of the foramen magnum and a low crista dorsalis basioccipitalis (Fig. 2B, F). In ventral view, the basioccipital is trapezoidal in shape and contacts the parabasisphenoid anteriorly and the posterior process of the pterygoid laterally for all its length. The parabasisphenoid, however, underlaps the anterior fifth of the basioccipital by means of a thin sheet of bone. Together with the pterygoid, the basioccipital forms two well-defined tubercula basioccipitale, which are buttressed from above by the exoccipital. The right exoccipital minutely contributes to the articular surface of the condylus occipitalis. The left exoccipital is damaged in this region, but a minor contribution seems plausible on this side as well. Two foramina basioccipitale are present on the ventral surface of the basioccipital, as in *Eubaena cephalica* (Rollot et al. 2018).

Exoccipital. The exoccipital forms the lateral wall of the cavum cranii, the lateral margin of the foramen magnum, the medial margin of the foramen jugulare anterius, and the medial wall of the recessus scalae tympani (Fig. 2A, F). The exoccipital closely approaches the condylus occipitalis and a minor contribution of the right exoccipital to the articular surface of the latter is visible. The same region is damaged for the left exoccipital and no contribution to the articular surface of the condylus occipitalis is visible. However, it seems plausible that a minor contribution was present on this side as well. The exoccipital contacts the supraoccipital dorsally, the opisthotic laterally, the pterygoid ventrolaterally and the basioccipital ventrally, and buttresses the tuberculum basioccipitale from above (Fig. 2F). Along the braincase wall, we are able to identify 4 small foramina on the medial surface of the exoccipital, but only one larger foramen on its external surface. Cranial nerves X, XI, and XII typically branch off the brain as multiple small branches that merge shortly after having left the brain (Soliman 1964; Kardong 2012). The arrangement observed in DMNH EPV.64550 perfectly illustrates this condition, in which 4 small hypoglossal nerve branches (XII) depart from the brain to enter the exoccipital through separate foramina, and merge within the latter bone to exit the skull by means of a single, enlarged foramen nervi hypoglossi. Unlike in *Eubaena cephalica* (Rollot et al. 2018), the exoccipitals and the basioccipital are clearly distinguishable in the CT scan, which suggests that this specimen likely belongs to a skeletally immature specimen.

Parabasisphenoid. The parabasisphenoid is a thick triangular bone that forms the ventral margin of the hiatus acusticus, the medial wall of the sulcus cavernosus,

and most of the floor of the cavum cranii (Figs 2B, 4). Ventrally, the parabasisphenoid broadly contacts the pterygoids laterally along straight sutures. The posterior contact with the basioccipital is transverse, but a surficial lamina of bone, likely homologous to the parasphenoid (Sterli et al. 2010), underlaps the basioccipital to yield a concavely curved suture. The parabasisphenoid otherwise contacts the prootic dorsolaterally. The rostrum basisphenoidale is flat and short, only representing about one third of the total length of the parabasisphenoid, and contacts the pterygoids ventrally (Fig. 2B). At the posterior limit of the rostrum basisphenoidale is the sella turcica, in which the two foramina arteria carotica interna are located (Fig. 4). The sella turcica is overhung by a tall dorsum sellae. Distinct retractor bulbi pits are not apparent. The short, wing-like clinoid processes, as seen in the 3D models, partially roof the sulcus cavernosus. The foramen posterius canalis nervi abducentis is located on the dorsal surface of the parabasisphenoid at about mid-length between the dorsum sellae and the posterior end of the bone. The canalis nervus abducentis is mostly formed by the parabasisphenoid, but the pterygoid forms the lateral margin of the right foramen arteria carotica interna, as in the pleurosternid *Pleurosternon bullockii* (Evers et al. 2020) and the early branching baenid *Arundelemys dardeni* (Evers et al. 2021). Ventrally, the parabasisphenoid forms the medial portion of most of the carotid groove, but the foramen posterius canalis carotici interni is only formed by the pterygoid, albeit extremely close to the pterygoid-parabasisphenoid suture. Shortly anterior to the foramen posterius canalis carotici interni, the canalis caroticus internus becomes the canalis caroticus basisphenoidalis, which is formed by the parabasisphenoid. The basiptyergoid process is absent.

Shell. The shell associated with the skull was reassembled, as it was disarticulated during burial. Although some bones are missing, those that remain are preserved in three dimensions (Figs 5, 6). The surface of the carapace is covered by numerous welts (Fig. 5A). Elongate welts are oriented anteroposteriorly, roughly parallel to the sagittal plane, and most densely arranged over the medial half of the costals. Most sulci can be traced with ease, with the exception of those in the nuchal area, which are difficult to discern. The shell is highly vaulted. The posterior margin of the carapace is scalloped and exhibits a broad pygal notch. The anterior margin is lightly scalloped as well. The skin-scutum sulcus runs along the margins of the visceral side of both carapace and plastron (Fig. 6).

The carapace likely consists of a nuchal, preneural, nine neural elements of which eight are interpreted as regular and one as supernumerary, a suprapygal, a pygal, eight pairs of costals, and twelve pairs of peripherals (Fig. 5A). The preneural and neural I have four sides and only contact costal I laterally. Neurons II–V are elongate, hexagonal, and have short anterolateral sides that contact the anterior costal. Neurons VI and VII are missing, but can be inferred to have been short, hexagonal elements. The surrounding elements suggest the presence of a short,

irregular neural that was squeezed between neurons VII and neural VIII, which we do not count as a full element of the neural series. Neural VIII is an elongate hexagon with short anterolateral sides. The suprapygal is crescent-shaped, has four contacts, and is about the size of the preneural. The pygal is much broader than long, forms much of the posterior margin of the shell, and exhibits a deep anterior concavity for articulation with the suprapygal. As in most baenids, costals I–IV are large elements, while costals V–VIII are reduced in size. Costal I is in contact with four peripherals and its rib inserts laterally into the fourth peripheral element. As the first costal rib seems to insert into the third peripheral universally among turtles (Joyce and Rollet 2020), this suggests that the small peripherals at the very front of the series are supernumerary elements relative to other turtles. To avoid propagating incorrect homology, we highlight the first pair of elements as supernumerary peripherals and start counting the regular peripheral series with the second element. As other *Denazinemys nodosa* shells only display three peripherals associated with costal I (Wiman 1933; Lichtig and Lucas 2015), this could be used as evidence for a distinct species. However, as the shell of baenids often exhibits irregular bone or scute arrangements (e.g., Wiman 1933; Gaffney 1972; Joyce and Lyson 2015), we interpret this as an anomaly until it can be consistently demonstrated among additional individuals. A peripheral count of 12 is reported for numerous baenids in the literature (e.g., Gaffney 1972) and is used as character evidence in baenid trees going back to Gaffney and Meylan (1988), but we find it doubtful that this characteristic exists in the first place (see Discussion below). The nuchal is a narrow, trapezoidal element that laterally contacts peripheral I on the right side only. The supernumerary peripheral is a small, triangular element that posteriorly contacts costal I on the left side only. As the axillary buttress reaches the very front of the shell, the posterior margin of peripheral I is V-shaped in cross section. The inguinal buttress is only partially preserved, but the posterior peripherals, at least peripherals VIII–XI, are flat in cross section.

The carapace was likely covered by five vertebrals, one pair of prepleurals, four pairs of pleurals, and twelve pairs of regular marginals, and one pair of supernumerary marginals (Fig. 5A). We are not able to determine the number of cervicals beyond one. Vertebral I is constricted anteriorly by the adjacent prepleurals. Vertebrals II–IV have six contacts, but are mostly square to rectangular in shape. Vertebral V is constricted posteriorly by marginals XII and contributes to the margin of the shell. The intervertebral sulci are located above neural I, III, V, and VIII, while the interpleural one are located above costals II, IV, VI, and VIII.

The plastron consists of an entoplastron and paired epi-, hyo-, meso-, hypo-, and xiphiplastra (Figs 5B, 6B). The anterior plastral lobe is short and triangular, the bridge region broad, and the posterior lobe short, but squared. The entoplastron is diamond-shaped in external view, but notably T-shaped in visceral view due to the development of a broad posterior entoplastral process. The mesoplastra

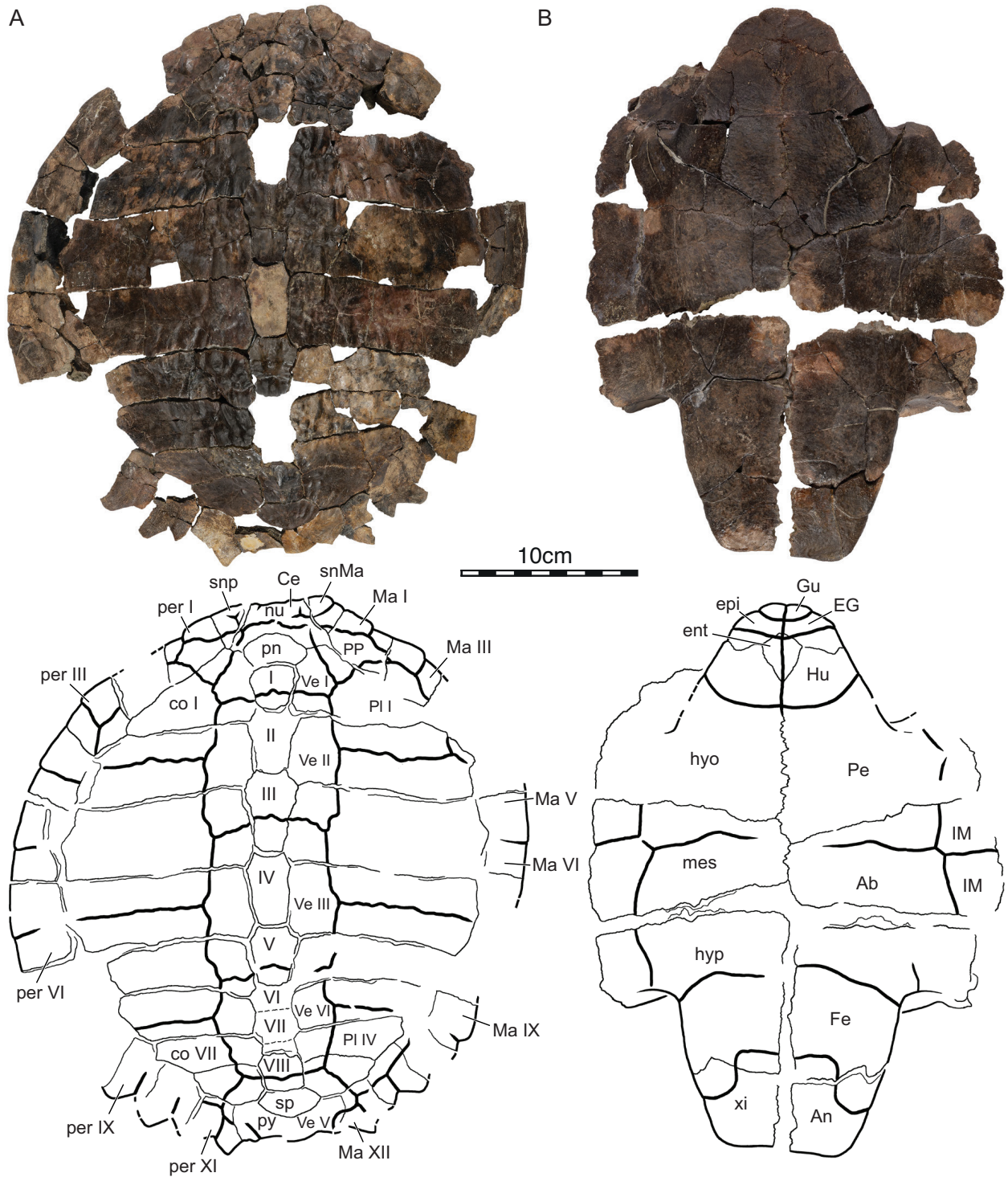


Figure 5. Photographs and interpretive line drawings of the exterior of the shell of DMNH EPV.64550. **A.** Dorsal view of the carapace, and **B.** Ventral view of the plastron. Abbreviations: Ab, abdominal scute; An, anal scute; Ce, cervical scute; co, costal; EG, extragular scute; ent, entoplastron; epi, epiplastron; Fe, femoral scute; Gu, gular scute; Hu, humeral scute; hyo, hyoplastron; hyp, hypoplastron; IM, inframarginal scute; Ma, marginal scute; mes, mesoplastron; nu, nuchal; Pe, pectoral scute; per, peripheral; PI, pleural scute; pn, preneural; PP, prepleural; py, pygal; snMa, supernumerary marginal; snp, supernumerary peripheral; sp, suprapygale; Ve, vertebral scute; xi, xiphoplastron. Neurals are given in Roman numerals.

show a broad, slightly asymmetric midline contact as in *Compsemys* (Gaffney, 1972). The hyoplastra form large, winglike axillary buttresses that reach anteriorly to contact the posterior corner of peripheral I and then articulate with nearly the full width of costal I from below.

The hypoplastra similarly form large, wing-like inguinal buttresses that articulate with a broad ridge formed at the contact of costals V and VI.

The plastron was likely once covered by paired gulars, extragulars, humerals, pectorals, abdominals, femorals,

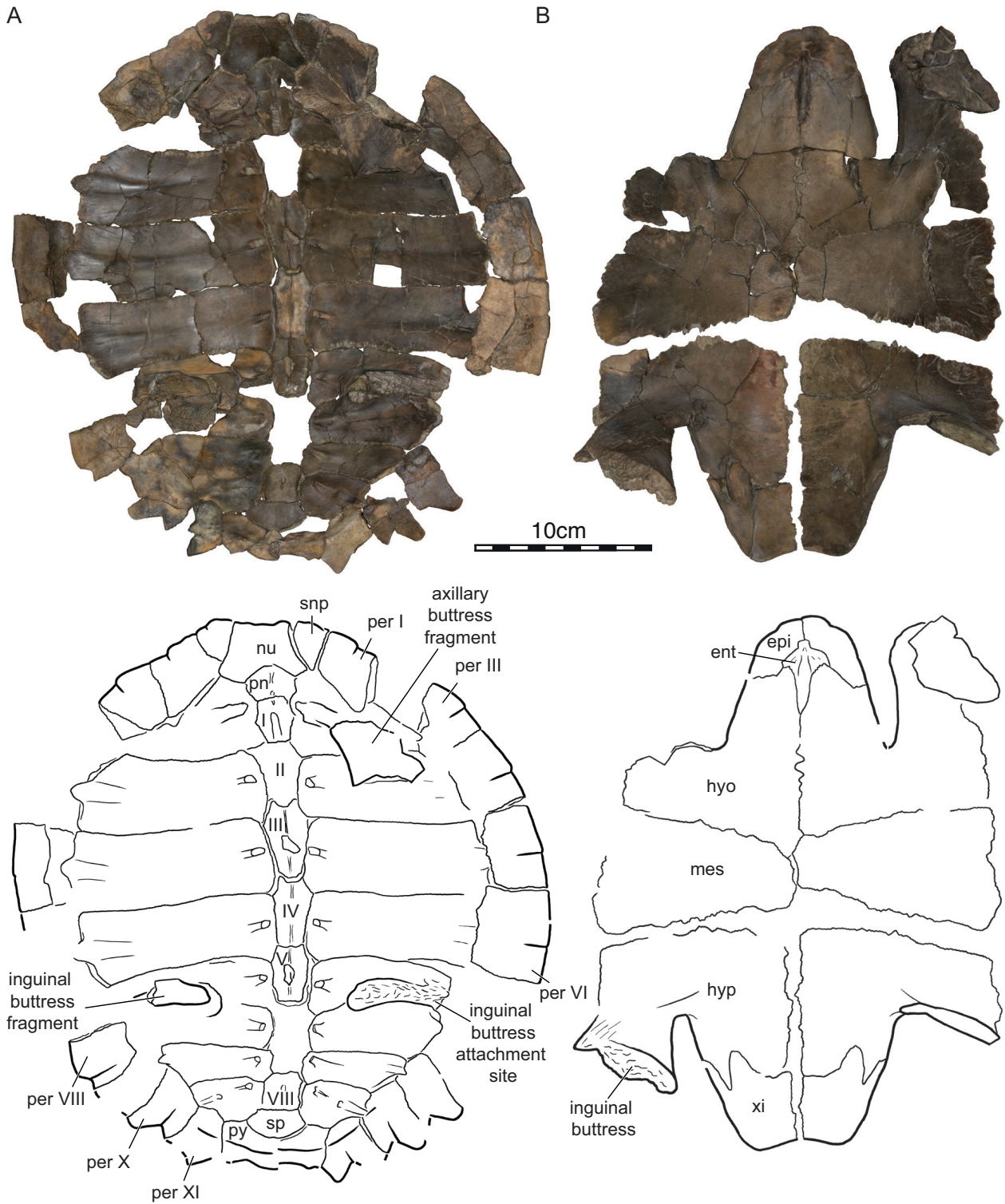


Figure 6. Three-dimensional renderings and interpretative drawings of the shell of DMNH EPV.64550 showing the inner part of the shell in **A**. Ventral view of the carapace, and **B**. Dorsal view of the plastron. Abbreviations: ent, entoplastron; epi, epiplastron; hyo, hyoplastron; hyp, hypoplastron; mes, mesoplastron; nu, nuchal; per, peripheral; pn, preneural; py, pygal; snp, supernumerary peripheral; sp, suprapygal; xi, xiphiplastron. Neurals are given in Roman numerals.

and anals (Fig. 5B). The gulars and extragulars are relatively small elements that are oriented transversely and have midline contacts with their counterparts. The extragular only barely covers the most anterior tip of the entoplastron. The humeral-pectoral sulcus is rounded and

located far behind the entoplastron. The femoral-anal sulcus is omega-shaped and crosses onto the hypoplastron. The exact number of inframarginals is not clear, but a complete series was certainly present that separated the carapacial scutes from contacting the plastral ones.

Discussion

Supernumerary peripherals in baenids

In the vast majority of turtles, 11 pairs of peripherals are developed, of which elements III through X are normally associated with costal ribs I through VIII. Notable exceptions are basal turtles from the Triassic, which often exhibit additional peripheral elements, although the exact count remains unclear, and kinosternids and carettochelyids, which universally exhibit only 10 pairs (Joyce 2007). The historic literature sometimes implies that baenids may have had 12 pairs of peripherals (e.g., Hay 1908; Gaffney 1972). Gaffney and Meylan (1988), therefore, more recently suggested that the presence of 12 peripherals may be a synapomorphy for the clade Baenodda (their Baenod). This character was retained in more recent phylogenetic analyses (e.g., Lyson and Joyce 2009a; Lively 2015; Joyce et al. 2020b; Rollot et al. 2022b). The unambiguous presence of 12 peripheral elements in DMNH EPV.64550 through the inclusion of additional elements to the front of the shell led us to review the distribution of this character. The best previously documented occurrence of supernumerary peripherals is available for the Campanian *Plesiobaena antiqua*. Brinkman (2003) documented for this taxon four well preserved shells, of which three exhibit 11 pairs of peripherals, of which the two most anterior elements are fused. The fourth individual, by contrast, exhibits on the left side of the shell what looks to be a subdivided eleventh peripheral. The marginal count remains at twelve. Hay (1908) otherwise documented 12 pairs of peripherals for the holotypes of “*Baena hatcheri*” (currently *Eubaena hatcheri*), “*Baena clara*” (currently *Baena arenosa*), and “*Baena emiliae*” (currently *Baena arenosa*). In all cases, however, the associated figures indicate that sutures are not actually preserved in the posterior parts of the shell, although a count of 13 marginals appears plausible. Hay (1908) also depicts “*Baena riparia*” (currently *Baena affinis*) as having 12 pairs of peripherals, but the relevant part of the shell is not actually preserved. We are therefore unaware of any baenid specimen that unambiguously documents the presence of twelve pairs of peripherals. At first sight, this conclusion appears somewhat surprising as baenids are extremely common in the fossil record, but this statement is put into perspective by the fact that baenids were riverine turtles with deterministic growth: smaller individuals with unfused shells typically disarticulate, which obscures their peripheral count, while adult specimens with better preservation potential exhibit fused shells. Our summary of the literature is insufficient to conclude that no baenid has twelve peripherals, but does highlight the fact that previous studies may have been guided by the presumption that twelve pairs may be present. We therefore deactivated the relevant character from our matrix and suggest that future research focus on this character.

Epipterygoid

The presence versus absence of a separately ossified epipterygoid is currently used as a character to resolve baenid relationships, but it remains unclear if the apparent variation is taxonomic, ontogenetic (as suggested by Brinkman (2003) based on variation seen in *Plesiobaena antiqua*), or the result of observational error. If variation is taxonomic, we would expect all, or at least most individuals of a species to display the same character state. If variation is ontogenetic (i.e., the result of fusion to a neighboring element), we would expect large specimens to consistently lack epipterygoids relative to younger individuals of the same species. Of course, it may also be possible that the epipterygoid only ossifies late in ontogeny. Finally, varying degrees of preservation could be the result of observational error, for instance, in that epipterygoids are incorrectly reported to be absent in crushed specimens, or that epipterygoids are apparent in CT scans, but look to be absent in external view of the same specimen. At present, we conclude that not enough data are available to resolve this question with confidence, but we suspect a mixture of all three factors.

Differences with BYU 19123

Lively (2016) provided figures and brief descriptions for two baenid skulls from the Kaiparowits Formation that he referred to *Denazinemys nodosa*. Although Lively (2016) was not able to observe many sutures in external view, we are able to confirm most of his observations for DMNH EPV.64550 using the μ CT scans available to us. However, we note some puzzling differences with BYU 19123, the second skull described by Lively (2016). First, while BYU 19123 has deep upper and lower temporal emarginations, those of DMNH EPV.64550 are relatively shallow. Second, while the orbits of DMNH EPV.64550 are oriented dorso-laterally, those of BYU 19123 are oriented more laterally. Third, while the parietal-frontal contact is oriented transversely in DMNH EPV.64550, it is oriented obliquely in BYU 19123. As a result, the parietals of DMNH EPV.64550 end bluntly and the frontals contact one another along their full length, but the parietals of BYU 19123 form enlarged anterior processes that protrude into the interorbital space and broadly hinder the frontals from contacting one another. Fourth, while DMNH EPV.64550 has jugals located just posteroventrally to the orbit, those of BYU 19123 are located posteriorly only. Fifth, while DMNH EPV.64550 has tall maxillae, those of BYU 19123 are notable slim. The depressor fossa behind the cavum tympani of DMNH EPV.64550 furthermore seems to be smaller than that of BYU 19123, but that appears to be the result of damage. The skull of DMNH EPV.64550 was found in close association among disarticulated shell elements referable to *Denazinemys nodosa* (see Geological Setting above). Notes on BYU localities from the Kaiparowits Formation are extremely limited to nonexistent, by contrast, preventing

confident association of the skull of BYU 19123 with the recovered shell material.

The morphological differences listed above suggest that the two skulls belong to two distinct species, thus questioning the attribution of one to *Denazinemys nodosa*. Although we are not able to further resolve this issue for the moment, we see two primary possibilities. On the one hand, as studies based on CT scans can retrieve sutures with confidence quite different from those apparent in external view (e.g., Rollet et al. 2022b), it is possible that the listed differences are errors in the interpretation of BYU 19123, perhaps amplified by differential damage to both specimens. If this is the case, attribution of either skull to *Denazinemys nodosa* is unproblematic. On the other hand, it is also possible that further study of BYU 19123 confirms the differences listed above, which either implies that the shell of *Denazinemys nodosa* is associated with two skull morphotypes, or that one of the two skulls simply does not belong to *Denazinemys nodosa*, even if it was found in close proximity to a diagnostic shell. The resulting parataxonomic conundrum (i.e., taxonomic instability caused by uncertain attributions of separate body parts to the same taxon) is typical for turtles, including baenids (e.g., Lyson and Joyce 2009a, b; Lyson et al. 2011). In contrast to BYU 19123, which was collected at least four decades ago without detailed field notes, we can personally vouch for the fact that the skull of DMNH EPV.64550 was found among the elements of a single shell, which resembles the holotype of *Denazinemys nodosa*, at a locality that otherwise did not yield abundant remains of other turtles. In addition, an unpublished skull found associated with another *Denazinemys nodosa* shell (RAM 31605 A.A. Farke, pers comm.) broadly confirms the morphology of DMNH EPV.64550. We, therefore, conclude this association to be the correct one until proven otherwise, with ambiguous association of skull and shell in BYU 19123.

Stratigraphic range of *Denazinemys nodosa*

Denazinemys nodosa was originally described based on a near complete shell from what is now classified as the Late Campanian De-na-zin Member at the top of the Kirtland Formation of New Mexico (Gilmore 1916; Sullivan and Lucas 2003, 2006). Soon after, a large sample of additional specimens was described by Wiman (1933), of which many likely originate from the underlying Late Campanian Hunter Wash Member of the Kirtland Formation (Sullivan et al. 2013). Sullivan et al. (2013) reported on the presence of *Denazinemys nodosa* in the Late Campanian Fruitland Formation of New Mexico, which regionally underlies the Kirtland Formation, but specimens were not figured. The reported presence of complete shells, however, provides us with confidence that the referred specimens are diagnostic of *Denazinemys nodosa*. Numerous additional specimens have since been described from New Mexico, but all fit within this stratigraphic range (Lucas and Sullivan 2006; Sullivan et al.

2013; Dalman and Lucas 2016; Lichtig and Lucas 2017). Hutchison et al. (2013) and Lively (2016) more recently described complete, diagnostic shells from the Late Campanian Kaiparowits Formation of Utah, which extend to temporal range of *D. nodosa* approximately 1 million years older (see Geological Settings above). The currently known range for this taxon based on diagnostic material is therefore restricted to the Late Campanian within a time interval of approximately 2.5 Ma (~76–73.5 Ma).

A number of additional remains have otherwise been referred to *Denazinemys nodosa* as well, including specimens from the Middle to Late Campanian Aguja Formation of Coahuila and Texas (Tomlinson 1997; Lehman et al. 2019; López-Conde et al. 2020), the Middle Campanian Wahweap Formation of Utah (Holroyd and Hutchison 2016), and the Lower Campanian Menefee Formation of New Mexico (Lichtig and Lucas 2015). In all cases, the material is highly fragmentary and diagnosed as *Denazinemys nodosa* by the presence of welts on carapace elements. Welts indeed are a highly conspicuous characteristic of *Denazinemys nodosa*, but they also occur in other baenids, including *Boremys pulchra* (Lambe 1902) from the Late Campanian of Alberta and Montana (e.g., Brinkman and Nicholls 1991), *Boremys grandis* Gilmore, 1935 from the Late Campanian of New Mexico (e.g., Sullivan et al. 2013), and *Scabremys ornata* (Gilmore 1935) from the Late Campanian of New Mexico. As these turtles appear to be closely related (see Phylogeny below), we note that this characteristic appears to be a synapomorphy of a clade, not an autapomorphy of *Denazinemys nodosa*. Sullivan et al. (2013) highlighted differences in shell surface texture between the above-listed taxa based on the complete shells that were available to them but similarly concluded that fragmentary remains cannot be identified to the species level. We, therefore, question the attribution of all Lower to Middle Campanian turtle fragments with welted carapace ornamentation to this taxon and await descriptions of more complete specimens from these older units.

Phylogeny

Our phylogenetic analysis resulted in 35 equally parsimonious solutions with 361 steps (see Suppl. material 2 for list of common synapomorphies). The strict consensus tree finds *Denazinemys nodosa* as the immediate sister to *Eubaena cephalica* (Fig. 7). This late Maastrichtian taxon was already previously found in the vicinity (Lyson et al. 2011, 2016, 2021) or as the immediate sister to *Denazinemys nodosa* (Lively 2015). This contrasts the results of Sullivan et al. (2013), who retrieved *D. nodosa* nested within a clade of Eocene baenids. Our analysis recovers two synapomorphies uniting the latter two taxa: orbits that are smaller than the height of the maxilla (character 4, state 1) and the presence of swollen maxillae (character 10, state 1). We are somewhat surprised by this result, as we had informally noticed many shape similarities between these two taxa during this project. However, this also may be an artifact

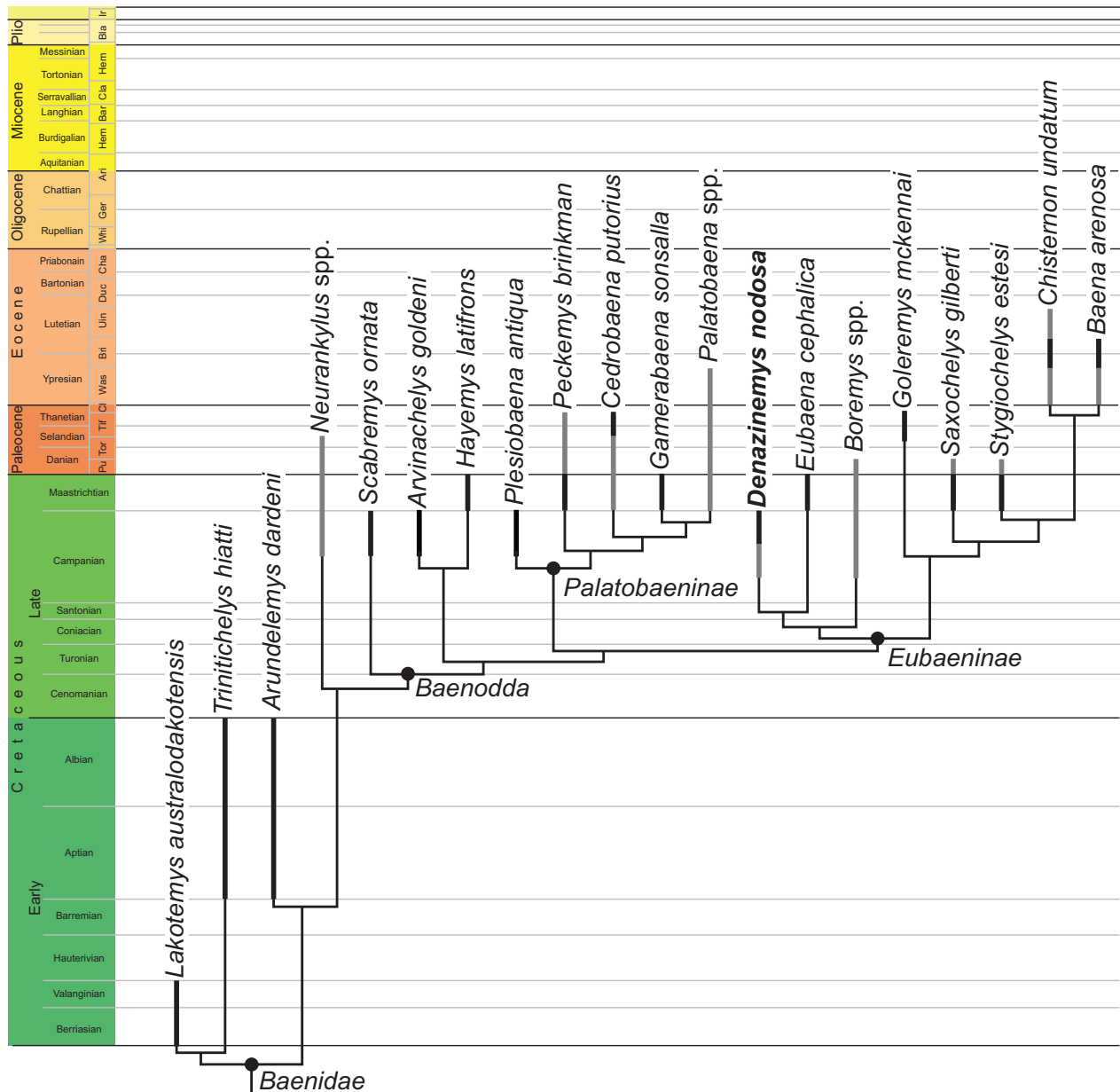


Figure 7. Strict consensus tree obtained in the phylogenetic analysis and mapped against the stratigraphic ranges for each taxon. Black lines indicate temporal distribution based on type material. Gray lines indicate temporal distribution based on referred material. For simplicity, taxa are referred to full time bins (i.e., the entire Maastrichtian or the entire late Campanian).

of sampling, as CT scans are also available for *Eubaena cephalica* (Rollot et al. 2018). Our hypothesis predicts that the shell of *Eubaena cephalica* should broadly resemble that of *Denazinemys nodosa*, but no shell material is known from the Maastrichtian that replicates the unique surface texture.

The sister group relationship of *Denazinemys nodosa* relative to *Eubaena cephalica* raises the question if the former may be ancestral to the latter. Although *Denazinemys nodosa* is thought to be restricted to the south-central portion of Laramidia and *Eubaena cephalica* to the north-central portion, we do not believe biogeography provides particularly strong evidence for or against this idea. However, our analysis indicates that *Denazinemys nodosa* has four autapomorphies, which would need to be secondarily lost if the latter is ancestral

to *Eubaena cephalica*, in particular the absence of a posterodorsal extension of the quadratojugal that crests the cavum tympani (character 19, state 1), presence of an epipterygoid (character 27, state 0), large mandibular condyles (character 60, state 1), and an anteriorly convex nasal/frontal suture (character 67, state 1). *Denazinemys nodosa*, therefore, does not fulfill the criteria of an ancestral metataxon for the moment (sensu Archibald 1994).

Our analysis retrieves *Boremys* spp. as the sister group to the clade formed by *Denazinemys nodosa* and *Eubaena cephalica*, broadly, once again, replicating previous results (Lyson et al. 2011, 2016, 2021; Lively 2015; see Sullivan et al. 2013 for different results). Three synapomorphies, which are common to all most parsimonious trees, are apparent: distinct scalloping of posterior shell margin (character 32,

state 2), gulars that are as large as the extragulars (character 46, state 1), and an anteriorly scalloped shell (character 51, state 1). An additional feature that unites these taxa is the distinct shell sculpturing consisting of raised welts, but it was not retrieved as a synapomorphy in the analysis.

An interesting insight gained by our analysis is the placement of *Goleremys mckennai*. This late Paleocene taxon had variously been found in previous analyses as a eubaenine (Lyson and Joyce 2009a, b; Lively 2015), a palatobaenine (Lyson et al. 2016), or a wildcard taxon (Lyson and Joyce 2010; Lyson et al. 2019; Rollot et al. 2022b). We, too, had initially found *Goleremys mckennai* to be a wildcard/rogue taxon, but then noticed that this may perhaps be the result of inconsistent scoring. After adjustment of the scorings of four characters (see Materials and Methods), we would expect this taxon to have a more stable placement within eubaenines. We now retrieve *Goleremys mckennai* as the sister taxon to the clade formed by *Baena arenosa*, *Chisternon undatum*, *Saxochelys gilberti*, and *Stygiochelys estesi*. Our result replicates the results of Lyson and Joyce (2009a, b), but not Lively (2015). The common synapomorphies for this arrangement formed by *G. mckennai* include the absence of a prefrontal exposure on the skull roof (character 13, state 2), a maximum combined width of parietals greater than their length (character 63, state 1) and the occipital condyle only formed by the basioccipital (character 101, state 1).

Our analysis retrieves the following 9 common synapomorphies uniting eubaenines: the absence of a palatine contribution to the triturating surface (character 8, state 0; 0/1 for *Denazinemys nodosa*), a reduced splenial (character 29, state 1; unknown for *Denazinemys nodosa*), the presence of preneurals (character 35, state 1; 0/1 for *Denazinemys nodosa*), the presence of two or more cervical scutes (character 38, state 2), the vertebral length greater than its width (character 39, state 2), the presence of a nuchal scute (character 40, state 1), the presence of prepleural scutes (character 41, state 1), a small suprapygal size (character 87, state 1), and an internal carotid artery canal that is anteriorly ossified and a foramen distalis nervi vidiani that is ventrally exposed (character 99, state 1).

Data availability

The specimen described herein is available to the public at the Denver Museum of Nature & Science (DMNS), Denver, Colorado, an approved repository for specimens from Bureau of Land Management (BLM) lands. The CT data and the 3D mesh models generated from it are available at MorphoSource (<https://www.morphosource.org/projects/000483670>).

Author contributions

WGJ, TRL, and JJWS designed the study. GES segmented cranial CT data and exported 3D mesh

models. LCG produced and exported the 3D mesh models of the shell. WGJ illustrated the shell and assembled figures. GES and WGJ assembled character matrix and conducted phylogenetic analyses. GES, TRL, YR, JJWS, LCG and WGJ prepared the manuscript and contributed to editing.

Competing interests

The authors declare that they have no conflict of interest.

Financial support

This research was supported by a grant from the Swiss National Science Foundation to WGJ (SNF 200021_178780/1), as well as the National Science Foundation (NSF-DEB-1947025) to TRL.

Acknowledgements

Specimen DMNH EPV.64550 was discovered by Geoff Lee and collected by JJWS under Bureau of Land Management (USA) permit UT11-011GS. Thanks to Alan Titus and Scott Foss for assistance with permits and additional thanks to Alan Titus for logistical support within GSENM. The specimen was expertly prepared in the DMNH labs by Jim Englehorn under the supervision of Bryan Small and Heather Finlayson. Additional mechanical preparation and repair of the shell was undertaken by Salvador Bastien for this study. Rick Wicker (DMNH) is thanked for professional specimen photography. The Kaiparowits Plateau, where the specimen was collected, is now protected as part of Grand Staircase-Escalante National Monument and managed by the BLM, is part of the ancestral lands of the Nuwuvi (Southern Paiute), Núu-ágha-tuvu-pú (Ute), Diné (Navajo), and Puebloan peoples. We are also grateful to Spencer Lucas and Juliana Sterli, who provided helpful comments that improved the quality of the manuscript.

References

- Archibald JD (1994) Metataxon concepts and assessing possible ancestry using phylogenetic systematics. *Systematic Biology* 43(1): 27–40. <https://doi.org/10.1093/sysbio/43.1.27>
- Archibald JD, Hutchison JH (1979) Revision of the genus *Palatobaena* (Testudines, Baenidae) with the description of a new species. *Postilla* 177: 1–19.
- Beveridge TL, Roberts EM, Ramezani J, Titus AL, Eaton JG, Irmis RB, Sertich JJW (2022) Refined geochronology and revised stratigraphic nomenclature of the Upper Cretaceous Wahweap Formation, Utah, U.S.A. and the age of early Campanian vertebrates from southern Laramidia. *Palaeogeography, Palaeoclimatology, Palaeoecology* 591: 1–22. <https://doi.org/10.1016/j.palaeo.2022.110876>

- Brinkman DB (2003) Anatomy and systematics of *Plesiobaena antiqua* (Testudines: Baenidae) from the mid-Campanian Judith River Group of Alberta, Canada. *Journal of Vertebrate Paleontology* 23(1): 146–155. [https://doi.org/10.1671/0272-4634\(2003\)23\[146:AASOPA\]2.0.CO;2](https://doi.org/10.1671/0272-4634(2003)23[146:AASOPA]2.0.CO;2)
- Brinkman DB, Hart M, Janniczky H, Colbert M (2006) *Nichollsemys baieri* gen. et sp. nov., a primitive chelonoid turtle from the late Campanian of North America. *Paludicola* 5: 111–124.
- Brinkman DB, Nicholls EL (1991) Anatomy and relationships of the turtle *Boremys pulchra* (Testudines: Baenidae). *Journal of Vertebrate Paleontology* 11(3): 302–315. <https://doi.org/10.1080/02724634.1991.10011400>
- Brinkman DB, Nicholls EL (1993) The skull of *Neurankylus eximius* (Testudines: Baenidae) and a reinterpretation of the relationships of this taxon. *Journal of Vertebrate Paleontology* 13(3): 273–281. <https://doi.org/10.1080/02724634.1993.10011509>
- Brinkman DB, Aquillon-Martinez MC, De Leon Dávila CA, Janniczky H, Eberth DA, Colbert M (2009) *Euclastes coahuilaensis* sp. nov., a basal cheloniid turtle from the late Campanian Cerro del Pueblo Formation of Coahuila State, Mexico. *PaleoBios* 28: 76–88.
- Cope ED (1873) On the extinct Vertebrata of the Eocene of Wyoming, observed by the expedition of 1872, with notes on the geology. *United States Geological Survey of the Territories* 6: 545–649.
- Dalman SG, Lucas SG (2016) Frederic Brewster Loomis and the 1924 Amherst College paleontological expedition to the San Juan Basin, New Mexico. In: Sullivan RM, Lucas SG (Eds) *Fossil Record 5*, New Mexico Museum of Natural History and Science Bulletin 74, Albuquerque, NM, USA, 61–66. <https://doi.org/10.56577/SM-2016.397>
- Evans J, Kemp TS (1976) A new turtle skull from the Purbeckian of England and a note on the early dichotomies of cryptodire turtles. *Palaeontology* 19: 317–324.
- Evers SW, Rollot Y, Joyce WG (2020) Cranial osteology of the Early Cretaceous turtle *Pleurosternon bullockii* (Paracryptodira: Pleurosternidae). *PeerJ* 8: e9454. <https://doi.org/10.7717/peerj.9454>
- Evers SW, Rollot Y, Joyce WG (2021) New interpretation of the cranial osteology of the Early Cretaceous turtle *Arundelemys dardeni* (Paracryptodira). *PeerJ* 9: e11495. <https://doi.org/10.7717/peerj.11495>
- Fassett JE, Steiner MB (1997) Precise age of C33N-C32R magnetic-polarity reversal, San Juan Basin, New Mexico and Colorado. In: *Mesozoic geology and paleontology of the Four Corners Region: New Mexico Geological Society, Forty-eighth Annual Field Conference, October 1–4, 1997*, 48, 239–247. <https://doi.org/10.56577/FFC-48.239>
- Gaffney ES (1972) The systematics of the North American family Baenidae (Reptilia, Cryptodira). *Bulletin of the American Museum of Natural History* 147: 241–320.
- Gaffney ES (1975) A phylogeny and classification of the higher categories of turtles. *Bulletin of the American Museum of Natural History* 155: 387–436.
- Gaffney ES (1979) The Jurassic turtles of North America. *Bulletin of the American Museum of Natural History* 162: 91–135.
- Gaffney ES, Hiatt R (1971) A new baenid turtle from the Upper Cretaceous of Montana. *American Museum Novitates* 2443: 1–9.
- Gaffney ES, Meylan PA (1988) A phylogeny of turtles. In: Benton MJ (Ed.) *The Phylogeny and Classification of the Tetrapods, Volume 1*. Oxford: Clarendon Press, 157–219.
- Gilmore CW (1916) Description of two new species of fossil turtles, from the Lance Formation of Wyoming. *Proceedings of the United States National Museum* 50(2137): 641–646. <https://doi.org/10.5479/si.00963801.50-2137.641>
- Gilmore CW (1919) Reptilian faunas of the Torrejon, Puerco, and underlying Upper Cretaceous formations of San Juan County, New Mexico. *United States Geological Survey Professional Paper*, 119, 1–68. <https://doi.org/10.3133/pp119>
- Gilmore CW (1935) On the Reptilia of the Kirtland Formation of New Mexico, with descriptions of new species of fossil turtles. *Proceedings of the United States National Museum* 83(2978): 159–188. <https://doi.org/10.5479/si.00963801.83-2978.159>
- Goloboff PA, Farris JS, Nixon KC (2008) TNT: A free program for phylogenetic analysis. *Cladistics* 24(5): 774–786. <https://doi.org/10.1111/j.1096-0031.2008.00217.x>
- Hay OP (1908) *The Fossil Turtles of North America*. Washington, DC: Carnegie Institution of Washington. (Publications 75.) 568.
- Holroyd PA, Hutchison JH (2016) Fauna and setting of the *Adelolophus hutchisoni* type locality of the Upper Cretaceous (Campanian) Wahweap Formation of Utah. *PaleoBios* 33: 1–9. <https://doi.org/10.5070/P9331031196>
- Hutchison JH (2004) A new eubaenine, *Goleremys mckennai*, gen. et sp. N., (Baenidae: Testudines) from the Paleocene of California. *Bulletin of the Carnegie Museum of Natural History* 36: 91–96. [https://doi.org/10.2992/0145-9058\(2004\)36\[91:ANEGMG\]2.0.CO;2](https://doi.org/10.2992/0145-9058(2004)36[91:ANEGMG]2.0.CO;2)
- Hutchison JH, Knell MJ, Brinkman DB (2013) Turtles from the Kaiparowits Formation, Utah. In: Titus AL, Loewen MA (Eds) *At the top of the Grand Staircase: the Late Cretaceous of southern Utah*, Indiana University Press, Bloomington, 295–318.
- Joyce WG (2007) Phylogenetic relationships of Mesozoic turtles. *Bulletin - Peabody Museum of Natural History* 48(1): 3–102. [https://doi.org/10.3374/0079-032X\(2007\)48\[3:PROMT\]2.0.CO;2](https://doi.org/10.3374/0079-032X(2007)48[3:PROMT]2.0.CO;2)
- Joyce WG, Lyson TR (2015) A review of the fossil record of turtles of the clade Baenidae. *Bulletin - Peabody Museum of Natural History* 56(2): 147–183. <https://doi.org/10.3374/014.056.0203>
- Joyce WG, Parham JF, Anquetin J, Claude J, Danilov IG, Iverson JB, Kear B, Lyson TR, Rabi M, Sterli J (2020a) *Testudinata*. In: de Queiroz K, Cantino PD, Gauthier JA (Eds) *Phylogeny – A Companion to the PhyloCode*, Boca Raton, CRC Press, 1045–1048.
- Joyce WG, Rollot Y (2020) An alternative interpretation of *Peltochelys duchastelii* as a paracryptodire. *Fossil Record* 23: 83–93. <https://doi.org/10.5194/fr-23-83-2020>
- Joyce WG, Rollot Y, Cifelli RL (2020b) A new species of baenid turtle from the Early Cretaceous Lakota Formation of South Dakota. *Fossil Record (Weinheim)* 23(1): 1–13. <https://doi.org/10.5194/fr-23-1-2020>
- Joyce WG, Anquetin J, Cadena EA, Claude J, Danilov IG, Evers SW, Ferreira GS, Gentry AD, Georgalis GL, Lyson TR, Perez-Garcia A, Rabi M, Sterli J, Vitek NS, Parham JF (2021) A nomenclature for fossil and living turtles using phylogenetically defined clade names. *Swiss Journal of Palaeontology* 140(5): 1–45. <https://doi.org/10.1186/s13358-020-00211-x>
- Kardong KV (2012) *Vertebrates: Comparative anatomy, function, evolution*, 6th edn. McGraw-Hill, New York, 794 pp.
- Klein IT (1760) *Klassifikation und kurze Geschichte der vierfüßigen Thiere*. Lübeck, Jonas Schmidt.
- Lambe LM (1902) New genera and species from the Belly River Series (mid-Cretaceous). *Contributions to Canadian Paleontology* 3: 25–81.
- Lehman TM, Wick SL, Brink AA, Shiller TA II (2019) Stratigraphy and vertebrate fauna of the lower shale member of the Aguja Formation (lower Campanian) in West Texas. *Cretaceous Research* 99: 291–314. <https://doi.org/10.1016/j.cretres.2019.02.028>

- Lichtig AJ, Lucas SG (2015) Turtles of the Lower Eocene San Jose Formation, San Juan Basin, New Mexico. *New Mexico Museum of Natural History and Science Bulletin* 67: 161–177. <https://doi.org/10.56577/SM-2014.226>
- Lichtig AJ, Lucas SG (2017) Sutures of the shell of the Late Cretaceous-Paleocene baenid turtle *Denazinemys*. *Neues Jahrbuch für Geologie und Paläontologie. Abhandlungen* 283(1): 1–8. <https://doi.org/10.1127/njgpa/2017/0622>
- Lipka TR, Therrien F, Weishampel DB, Jamniczky HA, Joyce WG, Colbert MW, Brinkman DB (2006) A new turtle from the Arundel Clay facies (Potomac Formation, Early Cretaceous) of Maryland, U.S.A. *Journal of Vertebrate Paleontology* 26(2): 300–307. [https://doi.org/10.1671/0272-4634\(2006\)26\[300:ANTFTA\]2.0.CO;2](https://doi.org/10.1671/0272-4634(2006)26[300:ANTFTA]2.0.CO;2)
- Lively JR (2015) A new species of baenid turtle from the Kaiparowits Formation (Upper Cretaceous, Campanian) of southern Utah. *Journal of Vertebrate Paleontology* 35(6): e1009084. <https://doi.org/10.1080/02724634.2015.1009084>
- Lively JR (2016) Baenid turtles of the Kaiparowits Formation (Upper Cretaceous: Campanian) of southern Utah, USA. *Journal of Systematic Palaeontology* 14(11): 891–918. <https://doi.org/10.1080/14772019.2015.1120788>
- López-Conde OA, Chavarría-Arellano ML, Montellano-Ballesteros M (2020) Nonmarine turtles from the Aguja Formation (Late Cretaceous, Campanian) of Chihuahua, Mexico. *Journal of South American Earth Sciences* 102: 102668. <https://doi.org/10.1016/j.jsames.2020.102668>
- Lucas SG, Sullivan RM (2006) *Denazinemys*, a new name for some Late Cretaceous turtles from the Upper Cretaceous of the San Juan Basin, New Mexico. *New Mexico Museum of Natural History and Science Bulletin* 35: 223–227.
- Lyson TR, Joyce WG (2009a) A new species of *Palatobaena* (Testudines: Baenidae) and a maximum parsimony and Bayesian phylogenetic analysis of Baenidae. *Journal of Paleontology* 83(3): 457–470. <https://doi.org/10.1666/08-172.1>
- Lyson TR, Joyce WG (2009b) A revision of *Plesiobaena* (Testudines: Baenidae) and an assessment of baenid ecology across the K/T boundary. *Journal of Paleontology* 83(6): 833–853. <https://doi.org/10.1666/09-035.1>
- Lyson TR, Joyce WG (2010) A new baenid turtle from the Upper Cretaceous (Maastrichtian) Hell Creek Formation of North Dakota and a preliminary taxonomic review of Cretaceous Baenidae. *Journal of Vertebrate Paleontology* 30(2): 394–402. <https://doi.org/10.1080/02724631003618389>
- Lyson TR, Joyce WG, Knauss GE, Pearson DA (2011) *Boremys* (Testudines, Baenidae) from the latest Cretaceous and early Paleocene of North Dakota: An 11-million-year range extension and an additional K/T survivor. *Journal of Vertebrate Paleontology* 31(4): 729–737. <https://doi.org/10.1080/02724634.2011.576731>
- Lyson TR, Joyce WG, Lucas SG, Sullivan RN (2016) A new baenid turtle from the early Paleocene (Torrejonian) of New Mexico and a species-level phylogenetic analysis of Baenidae. *Journal of Paleontology* 90(2): 305–316. <https://doi.org/10.1017/jpa.2016.47>
- Lyson TR, Saylor JL, Joyce WG (2019) A new baenid turtle, *Saxochelys gilberti*, gen. et sp. nov., from the uppermost Cretaceous (Maastrichtian) Hell Creek Formation: Sexual dimorphism and spatial niche partitioning within the most speciose group of Late Cretaceous turtles. *Journal of Vertebrate Paleontology* 39(4): e1662428. <https://doi.org/10.1080/02724634.2019.1662428>
- Lyson TR, Petermann H, Toth N, Bastien S, Miller IM (2021) A new baenid turtle, *Palatobaena knellerorum* sp. nov. from the lower Paleocene (Danian) Denver Formation of South-Central Colorado, U.S.A. *Journal of Vertebrate Paleontology* 41(2): e1925558. <https://doi.org/10.1080/02724634.2021.1925558>
- Ramezani J, Beveridge TL, Rogers RR, Eberth DA, Roberts EM (2022) Calibrating the zenith of dinosaur diversity in the Campanian of the Western Interior Basin by CA-ID-TIMS U-Pb geochronology. *Scientific Reports* 12(1): 1–20. <https://doi.org/10.1038/s41598-022-19896-w>
- Roberts EM (2007) Facies architecture and depositional environments of the Upper Cretaceous Kaiparowits Formation, southern Utah. *Sedimentary Geology* 197(3–4): 207–233. <https://doi.org/10.1016/j.sedgeo.2006.10.001>
- Roberts EM, Sampson SD, Deino AL, Bowring SA, Buchwaldt R (2013) The Kaiparowits Formation: a remarkable record of late Cretaceous terrestrial environments, ecosystems, and evolution in western North America. In: Titus AL, Loewen MA (Eds) *At the Top of the Grand Staircase: the late Cretaceous of Southern Utah*, Indiana University Press, Bloomington, IN, USA, 85–106.
- Rollot Y, Lyson TR, Joyce WG (2018) A description of the skull of *Eubaena cephalica* (Hay, 1904) and new insights into the cranial circulation and innervation of baenid turtles. *Journal of Vertebrate Paleontology* 38(3): e1474886. <https://doi.org/10.1080/02724634.2018.1474886>
- Rollot Y, Evers SW, Joyce WG (2021) A redescription of the Late Jurassic (Tithonian) turtle *Uluops uluops* and a new phylogenetic hypothesis of Paracryptodira. *Swiss Journal of Palaeontology* 140(1): 1–30. <https://doi.org/10.1186/s13358-021-00234-y>
- Rollot Y, Evers SW, Cifelli RL, Joyce WG (2022a) New insights into the cranial osteology of the Early Cretaceous paracryptodiran turtle *Lakotemys australodakotensis*. *PeerJ* 10: e13230. <https://doi.org/10.7717/peerj.13230>
- Rollot Y, Evers SW, Pierce SE, Joyce WG (2022b) Cranial osteology, taxonomic reassessment, and phylogenetic relationships of the Early Cretaceous (Aptian-Albian) turtle *Trinitichelys hiatti* (Paracryptodira). *PeerJ* 10: e14138. <https://doi.org/10.7717/peerj.14138>
- Soliman MA (1964) Die Kopfnerven der Schildkröten. *Zeitschrift für Wissenschaftliche Zoologie* 169: 216–312.
- Sterli J, Müller J, Anquetin J, Hilger A (2010) The parabasisphenoid complex in Mesozoic turtles and the evolution of the testudinate basicranium. *Canadian Journal of Earth Sciences* 47(10): 1337–1346. <https://doi.org/10.1139/E10-061>
- Sullivan RM, Lucas SG (2003) The Kirtlandian, a new land-vertebrate “age” for the Late Cretaceous of Western North America: New Mexico Geological Society, 54th Field Conference, Guidebook, 369–377. <https://doi.org/10.56577/FFC-54.369>
- Sullivan RM, Lucas SG (2006) The Kirtlandian land-vertebrate “age”-faunal composition, temporal position and biostratigraphic correlation in the nonmarine Upper Cretaceous of western North America. *New Mexico Museum of Natural History and Science Bulletin* 35: 7–29.
- Sullivan RM, Jasinski SE, Lucas SG (2013) Re-Assessment of late Campanian (Kirtlandian) turtles from the Upper Cretaceous Fruitland and Kirtland Formations, San Juan Basin, New Mexico, USA. In: Brinkman DB, Holroyd PA, Gardner JD (Eds) *Morphology and Evolution of Turtles*, Dordrecht, Netherlands, Springer, 337–387. https://doi.org/10.1007/978-94-007-4309-0_20
- Tomlinson SL (1997) Late Cretaceous and Early Tertiary turtles from the Big Bend region, Brewster County, Texas [dissertation]. Lubbock, TX, Texas Tech University, 194 pp.
- Wiman C (1933) Über Schildkröten aus der oberen Kreide in New Mexico. *Nova Acta Regiae Societatis Scientiarum Upsaliensis* 9(5): 1–34.

Supplementary material 1

Mesquite file of the character matrix used for the phylogenetical analysis

Authors: Gaël E. Spicher, Joseph J. W. Sertich, Léa C. Girard, Walter G. Joyce, Tyler R. Lyson, Yann Rollot
Data type: Character matrix

Copyright notice: This dataset is made available under the Open Database License (<http://opendatacommons.org/licenses/odbl/1.0>). The Open Database License (ODbL) is a license agreement intended to allow users to freely share, modify, and use this Dataset while maintaining this same freedom for others, provided that the original source and author(s) are credited.

Link: <https://doi.org/10.3897/fr.26.102520.suppl1>

Supplementary material 2

Common synapomorphies mapped onto the strict consensus tree

Authors: Gaël E. Spicher, Joseph J. W. Sertich, Léa C. Girard, Walter G. Joyce, Tyler R. Lyson, Yann Rollot
Data type: Phylogenetic

Copyright notice: This dataset is made available under the Open Database License (<http://opendatacommons.org/licenses/odbl/1.0>). The Open Database License (ODbL) is a license agreement intended to allow users to freely share, modify, and use this Dataset while maintaining this same freedom for others, provided that the original source and author(s) are credited.

Link: <https://doi.org/10.3897/fr.26.102520.suppl2>
